Macromolecules
ARTICLE

Macromolecules **2010**, *43*, 9787–9801 **9787**
DOI: 10.1021/ma102007e

Theoretical Investigation of Nano-Scale Organization in Blends of Semicrystalline/Semicrystalline Polymers by Small Angle X-ray Scattering

Finizia Auriemma,* Odda Ruiz de Ballesteros, and Claudio De Rosa

Dipartimento di Chimica "Paolo Corradini", Università di Napoli "Federico II", Complesso Monte Sant' Angelo, via Cintia, 80126 Napoli, Italy

Received August 30, 2010; Revised Manuscript Received October 23, 2010

ABSTRACT: A theoretical model has been derived for the calculation of small-angle X-ray scattering (SAXS) data from stacks of crystalline lamellae in which two or more kinds of lamellae are mixed within the same stack according to different statistical models, ranging from the fully random mode, to alternated one, up to block configurations. The model has been used to study the complex lamellar morphology which develops from melt in some blends obtained by mixing two semicrystalline samples of isotactic polypropylene (iPP) characterized by different degree of stereoreoregularity, similar molecular masses, and melting temperatures of ≈162 °C for the more stereoregular component iPP1 and ≈74 °C for the less stereoregular one iPP2. It is shown that for samples crystallized in conditions far from thermodynamic equilibrium, the observed SAXS intensity profiles may easily show absence of correlation peaks, associated with high amount of diffuse scattering, not easy to unravel. Using our theoretical approach we show that featureless SAXS intensity distribution may correspond to formation of disordered lamellar stacks with lamellae of the two components randomly mixed within the same stacks. The tendency of iPP1 and iPP2 to form mixed lamellar stacks with a random configuration provides clear evidence that the two components are miscible in the melt.

Introduction

Polymer blends of two semicrystalline polymers that are totally or partially miscible in the melt state have been widely studied to date.[1−3] In the field of binary blends, the number of systems that fulfill both requirements, i.e. miscibility in the melt and crystallization ability of the two components, is relatively small.[1a] The large interest for this category of blends derives on one hand from the large practical importance that have achieved some of these systems in widespread commercial applications,[3] as for instance the binary blends of linear and branched polyethylene or the blends between two semicrystalline chemically identical copolymers differing only in composition and, on the other hand, from the large number of different supermolecular structures and novel morphologies that may develop upon crystallization of the two components from a homogeneous melt.[1,2,4] The kind and the number of morphologies which are formed upon crystallization, in turn, depend on the miscibility of components, their individual ability to crystallize, and the composition of the mixtures. For instance, in the case of blends of crystalline polymers where crystallization of both components may proceed concurrently at the same temperature, formation of interpenetrating or even concentric spherulites has been observed.[1,2] In the case of binary blends of miscible components crystallizing sequentially, instead, where one component (A) crystallizes first at high temperatures forming spherulites, and the second component (B) crystallizes after at lower temperatures, the B component may form independent spherulites, independent lamellar stacks inside the spherulites of A component, or even the two components may form mixed lamellar stacks.[1,2] Interesting complex morphologies may also form in systems with a miscibility gap, for which liquid−liquid phase separation may become competitive with the crystallization rate of one or both components.[1]

The studies performed to date on semicrystalline blends with a high level of miscibility in the melt have been concentrated both on morphological aspects at micrometer and nanometer length scale. Among the techniques able to probe the structural organization of these blends at lamellar level small-angle X-ray scattering (SAXS) is very useful for the possibility to study the lamellar morphology of crystalline blends in detail, to extract precise information on the relative arrangement of the lamellae of the two components and amorphous phase.[4,5] However, the methods of analysis of SAXS data which have been used so far, have been namely based on the use of the one-dimensional autocorrelation function aided with additional experiments aimed at a confident evaluation of the relevant morphological parameters for the description of the lamellar structure, because of the intrinsic difficulty of using this classic approach especially in cases where the interference between the lamellar entities of the two components may not be neglected.

In this paper a theoretical model is derived for the calculation of small-angle X-ray scattering (SAXS) from stacks of lamellar crystals in which two or more kinds of lamellae are mixed within the same stack according to different statistical models, ranging from the fully random mode, to the model of alternating lamellae, up to block configurations, by explicitly taking into account the interference between lamellae of different kinds. The theoretical approach is tested in the case of a model blend of two isotactic polypropylene samples characterized by a different degree of stereoregularity and similar molecular mass and mass polydispersity index, synthesized using two different metallorganic catalysts. It is shown that our approach provides unique information related to the structural organization at nanometer length scale of the lamellae of the two components in the blends, and allows identifying the possible mechanism subtending the formation of different structures as a function of crystallization conditions and thermal history of samples, using standard SAXS measurements, even without scaling the intensity to an absolute scale (e.g., electrons/cm^3). We demonstrate that our approach may be applied also to systems crystallized in non controlled conditions, for which a wide distribution of lamellar thicknesses

*To whom correspondence should be addressed. Telephone: ++39 081 674341. Fax ++39 081 674090. E-mail: finizia.auriemma@unina.it.

Published on Web 11/10/2010

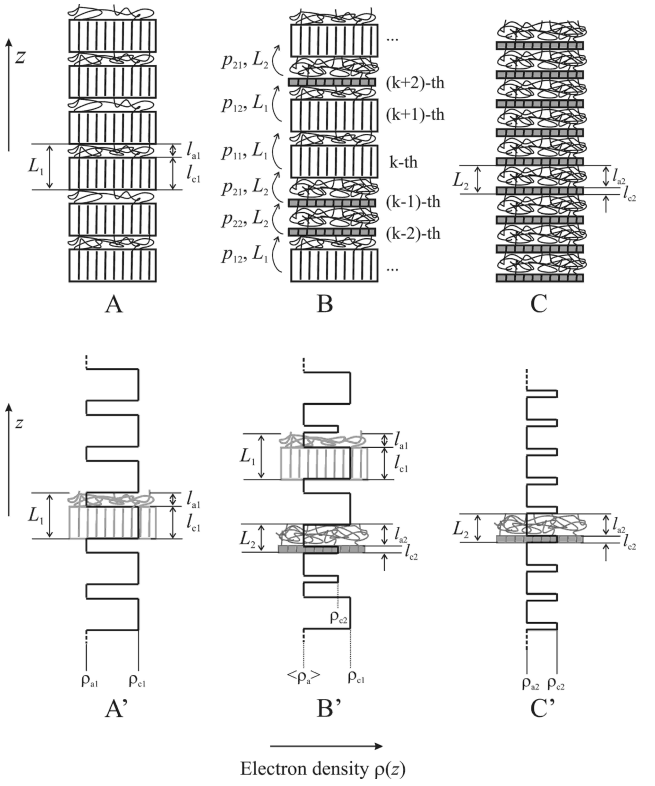

Figure 1. Idealized models of ordered (A, C) and disordered (B) arrays of crystalline lamellae and corresponding electron density profiles along z (A′−C′). Lamellae of thickness l_{c1} and l_{c2} and electron density ρ_{c1} and ρ_{c2} are separated by layers of amorphous chains of thickness l_{a1} and l_{a2}. The structural models A, C correspond to periodic stacks of lamellae with periodicity L_1 ($=l_{c1} + l_{a1}$) and L_2 ($=l_{c2} + l_{a2}$) respectively. In B, B′ the lamellae of kind 1 and 2 are mixed within the same stack and follow each other with the indicated probabilities p_{mn} and translation vectors L_m, in the assumption that the thickness and electron density of crystalline lamellae in the disordered stack are identical to those of pure components. The electron density of amorphous layers is ρ_{a1} and ρ_{a2} in the ordered lamellar stacks of pure components A and C, respectively, and it is assumed equal to the average value $\langle\rho_a\rangle = f_1'\rho_{a1} + f_2'\rho_{a2}$ for the disordered model B, with f_1' and f_2' the local volume fractions of the two components in the amorphous layers, not necessarily identical to the degree of inclusion of lamellae of the two components in the stack. The lateral dimensions of lamellae should be considered much higher than the average thickness of amorphous and crystalline layers, and the electron density in the planes normal to z are assumed to be constant and equal to $\rho(z)$.

are formed, and to blends where the constituting components have similar chemical structures, similar electron density, similar crystal structure, and close refractive indices, features that make the study of the lamellar organization of the two components in the blends very difficult with different techniques.

The Model

The present model is based on the classical assumption that stacks of lamellae may be approximated by a monodimensional array of alternating crystalline and amorphous layers of finite thickness and lateral dimensions much higher than the thicknesses of the two layers, arranged parallel each other[6] as shown in Figure 1A−C. Let l_{am} and l_{cm} the average thickness of amorphous and crystalline layers of m-th component in the blend, respectively, and ρ_{am}, ρ_{cm}, and $L_m = l_{am} + l_{cm}$ the corresponding electron density and long spacing, respectively. For a binary blend m = 1,2. The regular repetition along a direction (e.g., z) of crystalline lamellae of thickness l_{cm} alternating to amorphous layers of thickness l_{am} give rise to an ordered array of periodicity L_m as shown in Figure 1A,C. We assume that upon blending and successive crystallization, mixed stacks of lamellae of the two components are formed, and that these stacks may be modeled as monodimensionally disordered structures where lamellae of kind 1 and 2 follow each other along z according to a Markov process, as illustrated in Figure 1B. According to this model given that the kth lamella in the stack corresponds to the component m (thickness l_{cm}, electron density ρ_{cm}), the $(k+1)$-lamella follows at distance L_m separated by the kth amorphous layer (thickness l_{am}) and may be either of the same kind (m) with probability p_{mm}, or of different kind (n) with probability p_{mn}, all p_{mn}'s ($m, n = 1, 2$) being independent of k and the preceding $(k-1)$ lamellae already placed in the stack. In agreement with the supposed miscibility of the two components in the amorphous state, the electron density of the layers of amorphous chains in the disordered stack $\langle\rho_a\rangle$ is assumed to be equal to the average value of electron density of amorphous layers of pure components ρ_{a1} and ρ_{a2}, each weighted by the corresponding local volume fractions of the two components in the amorphous layers f_1' and f_2', not necessarily identical to the degree of inclusion of lamellae of the two components in the stack f_1 and f_2 respectively, according to equation

$$\langle\rho_a\rangle = f_1'\rho_{a1} + f_2'\rho_{a2} \tag{1}$$

For a two component system, the four conditional probabilities p_{11}, p_{12}, p_{21}, and p_{22} along with the fractions f_1 and f_2 of lamellae of kind m included in the stack are not independent, but they are bound by the set of eqs 2, for a total number of independent parameters equal to two:

$$\begin{cases} \sum_m f_m = 1 \Rightarrow f_1 + f_2 = 1 \\ \sum_m f_m p_{mn} = f_n \Rightarrow f_1 p_{11} + f_2 p_{21} = f_1; \quad f_1 p_{12} + f_2 p_{22} = f_2 \\ \sum_n p_{mn} = 1 \Rightarrow p_{11} + p_{12} = 1; \quad p_{21} + p_{22} = 1 \end{cases} \tag{2}$$

Notice that completely random arrangements of lamellae of kind (...12212212112...) correspond to setting $p_{mm} = p_{mn} = p$ and imply that the fraction f_m of lamellae of kind m is numerically coincident with p; perfectly alternating arrangements of lamellae of the kind (...121212...) correspond to setting $p_{mn} = 1$ for $m \neq n$, so that the probability that consecutive lamellae are of the same kind p_{mm} is equal to zero and $f_1 = f_2 = 0.5$; arrays of lamellae with a block configuration of kind (...1111122222...) correspond to setting $p_{mm} = 1$ so that the values of conditional probabilities p_{mn} for $m \neq n$ are equal to zero, and the fraction of lamellae of kind 1 or 2 in the crystalline arrays, f_m, becomes the independent parameter. In general, similar values of p_{mm} and p_{mn} correspond to nearly random configurations, values of p_{mn} for $m \neq n$ close to 1 correspond to alternating configurations, whereas values of p_{mm} close to 1 correspond to block-like configurations. Notice that only for the perfect block configuration (i.e., $p_{11} = p_{22} = 1$) the scattered intensity from different blocks contribute additively to the total intensity, whereas in all other cases the interference terms between different lamellae in the stack (i.e., from lamellae with different lamellar thickness and/or electron density) may not be neglected.

In the general case, once set the values of a couple of independent p_{mn} parameters, e.g. p_{11} and p_{22}, the fraction of lamellae of kind m may be calculated by equations

$$f_1 = \frac{1 - p_{22}}{2 - p_{11} - p_{22}} \tag{3}$$

$$f_2 = 1 - f_1 \tag{3'}$$

In other terms, the model of Figure 1B, corresponds to a monodimensional lattice where lamellae of two different kinds are arranged parallel each other within the same stack, and the mixing of these lamellae follows a Markov process as given by the

transition probabilites p_{mn}'s and the set of different translation vectors L_m's. In this model, for the sake of simplicity, the thicknesses of crystalline and amorphous layers, and the electron density of crystals have been assumed identical to those of pure components, even though these assumptions may be easily left out. It is worth noting that the assumption that electron density of amorphous layers is given by a weighted average of electron density of amorphous layers of pure components (eq 1) is a direct consequence of the hypothesized miscibility of the two components in the melt and amorphous state, which is likely the condition *sine qua non* (necessary but not sufficient) for formation of mixed lamellar stacks.[1] Also the assumption that the electron density of crystalline lamellae of pure components is kept by the lamellae of each component within the mixed stacks is quite reasonable, and corresponds to the experimental evidence that crystalline molecular complexes of different polymers (polymer cocrystals) are very rare. Instead, the assumption that the thickness of amorphous and crystalline layers of pure components is retained in the disordered lamellar stacks upon blending is not necessary and indeed, the mathematical formula here derived for the calculation of SAXS intensity from disordered lamellar stacks is more general and the above assumption is not considered.

The mathematical problem of evaluating the X-ray diffraction intensity scattered by monodimensionally disordered structures has been dealt by several authors,[7,8] and the derived formulas have been used to study the diffraction at wide angle from layered compounds as natural silicates[7c] or metal halides,[8] which present quite frequently stacking fault disorder consisting in the stacking along one-direction of structural layers of different nature and/or with different translation vectors. Within this contest we make use of the general matrix formalism given by Allegra in ref 8d to derive analytical formulas for the calculation of small-angle X-ray scattering intensity profiles in the case of disordered structural models with lamellae of different kinds stacked disorderly along one direction through different translation vectors according to a Markov process of the kind shown in Figure 1B.

Let the kth lamella in a stack be of kind m and placed at height z_k along z (thickness l_{cm}, electron density ρ_{cm}). The structure factor V_k of this lamella corresponds to the Fourier transform of a step function $S_k(z)$, defined as

$$S_K(z) = \begin{cases} \rho_{cm} - \langle \rho_a \rangle = \Delta\rho_m & \text{for } 0 < (z - z_k) < l_{cm} \\ 0 & \text{for } (z - z_k) < 0 \text{ and } (z - z_k) > l_{cm} \end{cases} \tag{4}$$

and is given by the integral

$$V_k(q) = \int_{z_k}^{z_k + l_{cm}} \Delta\rho_m \exp(-iqz)\, \mathrm{d}z = \exp(-iqz_k) V_{(m)} \tag{5}$$

where $q = 2\pi(2(\sin\theta)/\lambda)$ is the scattering vector with θ one-half of diffraction angle, $\Delta\rho_m$ is the contrast, i.e., the difference in electron density between the crystalline and amorphous phase, and the symbol $V_{(m)}$ denotes that the lamella in question is of kind m, and represents the structure factor of a lamella of kind m placed at the origin given by

$$V_{(m)} = \frac{\Delta\rho_m}{qi}(1 - \exp(-iql_{cm})) \tag{6}$$

The scattering amplitude $A(q)$ from a parallel stack of lamellae including N lamellae is given by

$$A(q) = \sum_{k=1}^{N} V_k(q) \tag{7}$$

whereas the general expression for the average scattering intensity $I(q)$ from a single disordered stack is given by

$$I(q) = \langle \sum_{k=1}^{N} V_k(q) \sum_{k'=1}^{N} V^*_{k'}(q) \rangle = \sum_{k=1}^{N} \langle V_k(q) V^*_k(q) \rangle + \sum_{k=1}^{N} \sum_{l=1}^{N-k} \langle V_k(q) V^*_{k+l}(q) \rangle + \langle V_{k+l}(q) V^*_k(q) \rangle \tag{8}$$

In eq 8 the symbol V_k* indicates the complex conjugate of the k-th lamellar structure factor (eq 5) whereas the symbol $\langle ... \rangle$ denotes the average of the square-modulus of scattering amplitude $A(q)$ (eq 5) over all possible configurations in the sequence of lamellae in the stack responding to the given statistics dictated by the Markov process. In the right-most part of eq 8 the first term corresponds to the sum of the self-interference term of the crystalline layers, whereas the second term is a double sum which may be broken into the contributions to the intensity due to interference between first neighboring layers (for $l = 1$), second neighboring layers ($l = 2$) etc. Notice that in replacing the average of square-modulus of $A(q)$ with the sum of averages of the interference terms of the lamellae we have implicitly recognized the fact that disorder within the stacks is not correlated.

Let us first evaluate the self-interference term in eq 8. This term is given in explicit by:

$$\sum_{k=1}^{N} \langle V_k(q) V^*_k(q) \rangle = N \sum_m f_m V_{(m)} V^*_{(m)}(q, l_{cm}) = N\mathbf{V}\mathbf{F}\mathbf{V}^{*T} \tag{9}$$

In the right-most part of eq 9, we have used a matrix formalism given by Allegra in ref 8d for which $\mathbf{V}$ is the row vector of structure factors $V_{(m)}$, $\mathbf{V}^{*\mathrm{T}}$ is the corresponding transpose conjugate matrix, $\mathbf{F}$ the diagonal matrix whose elements are the fraction of lamellae of kind m in the stack, given by:

$$\begin{cases} \mathbf{V} = |\, V_{(1)} \quad V_{(2)} \,|; \quad \mathbf{V}^{*T} = \begin{vmatrix} V^*_{(1)} \\ V^*_{(2)} \end{vmatrix} \\ \mathbf{F} = \begin{vmatrix} f_1 & 0 \\ 0 & f_2 \end{vmatrix} \end{cases} \tag{10}$$

Next we evaluate the contributions to the intensity due to interference between first neighboring layers, still resorting to the matrix formalism of ref 8d, as

$$\sum_k \langle V_k(q) V^*_{k+1}(q) \rangle + \langle V_{k+1}(q) V^*_k(q) \rangle = (N-1)\langle V_k(q) V^*_{k+1}(q) \rangle + \langle V_{k+1}(q) V^*_k(q) \rangle = (N-1)(\mathbf{VFMV}^{*T} + \mathbf{VFM}^*\mathbf{V}^{*T}) \tag{11}$$

In eq 11, we have considered that there are (N − 1) first neighboring layers, whose contribution to the intensity is given by averaging over all possible sequences of first neighboring layers, whereas in the right-most part of this equation $\mathbf{M}$ is a 2×2 matrix defining the possible translation vectors between alike and unlike first neighboring lamellae according to the assumed statistics, and $\mathbf{M}^*$ the matrix of the corresponding complex conjugates. More precisely

$$\begin{cases} \mathbf{M} = (1-\gamma) \begin{vmatrix} p_{11}\langle \exp(-iqL_1) \rangle & p_{12}\langle \exp(-iqL_1) \rangle \\ p_{21}\langle \exp(-iqL_2) \rangle & p_{22}\langle \exp(-iqL_2) \rangle \end{vmatrix} \\ \mathbf{M}^* = (1-\gamma) \begin{vmatrix} p_{11}\langle \exp(iqL_1) \rangle & p_{12}\langle \exp(iqL_1) \rangle \\ p_{21}\langle \exp(iqL_2) \rangle & p_{22}\langle \exp(iqL_2) \rangle \end{vmatrix} \end{cases} \tag{12}$$

In eq 12, a Bernoulli type distribution of the number of lamellae in the stack has been assumed,[9] with $(1 - \gamma)$ the probability that at

any new deposition of a lamella on the growing stack the growth process is continued, and γ the probability that the growth is terminated, the value of γ being assumed independent of the number of already deposited layers. With this assumptions the average number of lamellae in the stack $\langle N\rangle$ is related to the value of γ by the relation $\gamma = 1/\langle N\rangle$ and the general expression of scattered intensity given by eq 8 should be intended as the average over all possible lengths N of the stacks.

Similarly, the contributions to the intensity due to pairs of lth neighboring lamellae is given by

$$\begin{aligned}\langle \sum_{k=1}^{N} \langle V_k(q)V^*_{k+l}(q)\rangle + \langle V_{k+l}(q)V^*_k(q)\rangle\rangle_N \\ = \langle N-l\rangle\langle V_k(q)V^*_{k+l}(q)\rangle + \langle V_{k+r}(q)V^*_l(q)\rangle \\ = \langle N-l\rangle[\mathbf{VFM}^l\mathbf{V}^{*T} + \mathbf{VF}(\mathbf{M}^*)^l\mathbf{V}^{*T}] \end{aligned} \quad (13)$$

As a result, introducing the matrix formalism given in rightmost parts of eq 9 and 13 in eq 8, it may be shown (see ref 8d) that the overall scattered intensity may be calculated as:

$$\frac{I(q)}{\langle N\rangle} = \mathbf{VF}[-\mathbf{E}_2 + (\mathbf{E}_2 - \mathbf{M})^{-1} + (\mathbf{E}_2 - \mathbf{M}^*)^{-1}]\mathbf{V}^{*T} \quad (14)$$

where $\mathbf{E}_2$ is the unit matrix of order 2.

The multiplication matrix scheme in eq 14 contains self-product terms of the structure factors of crystalline lamellae $V_{(m)}V^*_{(m)}$ and cross product terms $V_{(m)}V^*_{(n)}$ with $m \neq n$, which may be formally written as

$$\begin{cases} V_mV_m^* = \dfrac{\Delta\rho_m}{q}[2 - \exp(-iql_{cm}) - \exp(iql_{cm})] \\ V_mV_n^* = \dfrac{\Delta\rho_m\Delta\rho_n}{q^2}[1 - \exp(-iql_{cm}) - \exp(iql_{cn}) + \exp(-iql_{cm})\exp(iql_{cn})] \end{cases} \quad (15)$$

In the hypothesis that the distribution of lamellar thickness is a Gaussian function centered at l_{cm} (l_{cn}) with standard deviation σ_{cm} (σ_{cn}), eqs 15 become:

$$\begin{cases} V_mV_m^* = \dfrac{\Delta\rho_m}{q}[2 - \langle\exp(-iql_{cm})\rangle - \langle\exp(iql_{cm})\rangle] \\ V_mV_n^* = \dfrac{\Delta\rho_m\Delta\rho_n}{q^2}[1 - \langle\exp(-iql_{cm})\rangle - \langle\exp(iql_{cn})\rangle \\ \qquad + \langle\exp(-iql_{cm})\rangle\langle\exp(iql_{cn})\rangle] \end{cases} \quad (16)$$

where the average terms $\langle\exp(-iql_{cm})\rangle$ are given by

$$\langle\exp(-iql_{cm})\rangle = \exp\left[-\frac{\sigma_{cm}{}^2q^2}{2}\right]\exp(-iql_{cm}) \quad (17)$$

In eq 12, the averages terms $\langle\exp(-iqL_m)\rangle$ may be evaluated assuming that also the distribution of thickness of amorphous regions is given by a Gaussian function centered at l_{am} with standard deviation σ_{am}. Therefore, the average terms $\langle\exp(-iqL_m)\rangle$ correspond to the Fourier transform of this Gaussian distribution function given by:

$$\langle\exp(-iqL_m)\rangle = \exp\left[-\frac{(\sigma_{cm}^2 + \sigma_{am}^2)q^2}{2}\right]\exp[-iq(l_{cm} + l_{am})] \quad (18)$$

with $\langle\exp(iqL_m)\rangle$ the corresponding complex conjugate of eq 18.

In general for a multimodal distribution of thicknesses of amorphous layers modeled as a sum of Gaussian functions centered around average thickness values l_{am1}, l_{am2}, l_{am3}... l_{amj}... with $j = 1, 2, 3, \ldots J$, corresponding to standard deviations σ_{am1}, σ_{am2}, σ_{am3}... σ_{amj}... the term $\langle\exp(-iqL_m)\rangle$ may be calculated as

$$\langle\exp(-iqL_m)\rangle = \exp\left[-\frac{(\sigma_{cm}{}^2)q^2}{2}\right]\exp[-iq(l_{cm})]\left[\sum_{j=1}^{J}\beta_j\exp\left[-\frac{(\sigma_{amj}{}^2)q^2}{2}\right]\exp[-iq(l_{amj})]\right] \quad (19)$$

with J the number of possible average thicknesses of amorphous layers separating consecutive crystalline lamellae in the disordered stack, and β_j the fraction of amorphous layers with thickness l_{amj}.

It is worth noting that eq 14 is widely more general and may be easily extended to the case where a multimodal distribution of crystalline lamellar thickness is also present, by increasing the ordered of **V**, **F**, **M**, **M***, and **V*** matrices in a right straightforward manner.

Chart 1. Structure of C_2-Symmetric (1) and C_1-Symmetric Zirconocene (2) Precatalysts

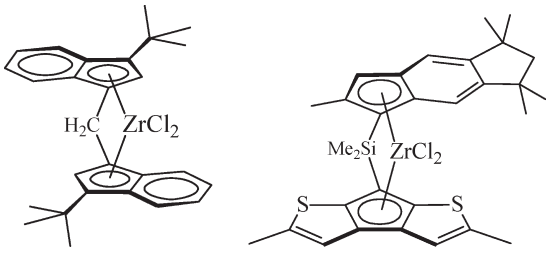

1 **2**

Table 1. Viscosity Average Molecular Masses (M_v), Content of Triad Stereo-Sequences and Melting Temperatures (T_m) of the iPP Samples Prepared with Catalysts of Chart 1[a]

sample	catalyst	M_v[b]	*mm* (%)[c]	*mr* (%)[c]	*rr* (%)[c]	T_m (°C)[d]
iPP1	**1**/MAO	195 700	98.54	0.98	0.49	162
iPP2	**2**/MAO	162 000	71.4	19.1	9.53	74

[a] No or negligible regioerrors (2,1 insertions) could be observed in the ^{13}C NMR spectra of the samples.[10−13] [b] From the intrinsic viscosities through the equation $[\eta] = K(M_v)^{\alpha}$, with $K = 1.93 \times 10^{-4}$ and $\alpha = 0.74$.[15] [c] From ^{13}C NMR analysis. [d] Measured from DSC scans at heating rate of 10 °C/min on as polymerized samples.[14]

Experimental Section

For the preparation of binary blends of this study we have utilized two well characterized samples of isotactic polypropylene (iPP) having different stereoregularity, synthesized with the two highly regiospecific C_2- and C_1-symmetric metallocene complexes shown in Chart 1, activated with methylalumoxane (MAO), as explained elsewhere.[10−13] The samples have similar molecular mass, mass polydispersity index around 2, and are denominated iPP1 and iPP2.[14] The main characteristics of these samples are collected in Table 1.

The sample iPP1 has been synthesized using the C_2-symmetric complex **1** *rac*-H_2C(3-*tert*-butylindenyl)$_2ZrCl_2$ of Chart 1,[10,11] is highly stereoregular, with a concentration of sterreodefect essentially consisting of *rr* triads equal to 0.49 mol %, and shows high melting temperature $T_m \approx 160$ °C.[14] The sample iPP2 has been synthesized using the C_1-symmetric *ansa*-zirconocene complex **2**,[12,13] shows a high concentration of stereodefects with a concentration of *rr* triads of 9.53 mol %, and low melting temperature $T_m \approx 74$ °C.

Five iPP1/iPP2 blends of composition 10/90, 30/70, 50/50, 70/30, and 90/10 w/w have been prepared. The different blend samples are designated as iPP1-*x*/iPP2-*y*, with x and y the weight percent of iPP1 and iPP2, respectively. The blends have been prepared from

solution by dissolving weighed amounts of the two components in refluxing xylene (bp 140 °C) for 1 h up to obtain homogeneous and transparent solutions and then precipitating the mixture into an excess (3:1) of cold methanol. The precipitated powders have been washed with methanol, filtered and dried under vacuum at 60 °C for 1 day. About 1 wt % of 2,6-di-*tert*-butyl-4-methylphenol has been added in the methanol as an antioxidant. At the end of dry process the precipitated mixtures have been weighed denoting a weight loss of the mixed polymers less than 1% in all cases.

Compression molded films of pure components and blends, with uniform thickness of about 1−2 mm, have been prepared by melting the dry-precipitated powders at 180 °C for 10 min under a press and cooling to room temperature under noncontrolled conditions, using a flux of cold water within the hot plates. The pressure applied under the press has been regulated in such a way to avoid preferred orientation in the film, and at same time to minimize formation of nanovoids and surface imperfections. The so obtained melt pressed films have been used for SAXS, wide-angle X-ray scattering (WAXS) and DSC measurements.

SAXS data have been collected using an evacuated high performance SAXS instrument "SAXSess" (Anton Paar KG, Graz, Austria), which is a modification[16] of the so-called "Kratky compact camera".[17] Data collection has been performed in the slit collimation configuration with SAXSess camera attached to a conventional X-ray source (Cu Kα, wavelength $\lambda = 1.5418$ Å). The scattered radiation has been recorded on a BAS-MS imaging plate (Fujifilm) in a configuration which allows recording simultaneous WAXS and SAXS data and processed with a digital imaging reader (Fuji BAS 1800), at a resolution in the small angle region of ≈60 nm ($=2\pi/q_{min}$, with q_{min} the minimum accessible value of scattering vector permitted by our collimation set up, equal to 0.1 nm^{-1} and $q = 4\pi\sin\theta/\lambda$, 2θ being the scattering angle). After subtraction for dark current, the empty sample holder, and a constant background due to thermal density fluctuations, the slit smeared data in the SAXS region (for $q < 4\ nm^{-1}$) have been deconvolved with the primary beam intensity distribution using the SAXSquant 2.0 software to obtain the corresponding pinhole scattering (desmeared) intensity distribution.

In the assumption that SAXS intensity probes heterogeneities arising from a simple two phase structure at nanometer length scale, the SAXS desmeared data, after subtraction of the residual background intensity (approximated as a constant I_b) has been extrapolated to high q values with the aid of the Porod law,[18] in the hypothesis of no diffuse boundary between crystalline and amorphous layers, i,e. by fitting the experimental data in the high q region ($1.5\ nm^{-1} < q < 3\ nm^{-1}$) with equation:

$$\lim_{q \to \infty} (I_{obs}(q) - I_b) = K_p q^{-4} \tag{20}$$

where K_p is a quantity proportional to the Porod constant P through a factor K due the fact that our intensity is in relative units.

For the extrapolation to $q = 0$ of SAXS desmeared data we have used the Debye−Beuche equation.[19] Since our blends are isotropic systems with no preferred orientation of the crystals, the total scattered intensity I inclusive of the extrapolated data at low and high q values has been transformed into one-dimensional intensity by Lorenz factor equal to $4\pi(2(\sin\theta)/\lambda)^2 = q^2/\pi$.[18] From these data the scattering invariant Q (in relative K units)[18] has been calculated as:

$$Q = \frac{1}{2\pi^2}\int_0^\infty Iq^2\,dq \tag{21}$$

The wide angle regions recorded simultaneously with SAXS data has not been "desmeared", because the used software works in the infinite slit length approximation and, at high q, this approximation may not be used. However, we have checked that the position of Bragg reflections, the width at half-height of the peaks and the overall shape of diffraction profiles for $q > 7\ nm^{-1}$ are not greatly affected by use of the slit collimation configuration instead of the pinhole geometry. This has been checked by collecting wide-angle X-ray diffraction profiles of selected samples with Ni filtered Cu Kα radiation using an automatic Philips diffractometer. The indices of crystallinity (x_c) determined from the X-ray powder diffraction profiles obtained with the two silt configurations are identical within the experimental error (3−5%). They have been evaluated by the ratio between the crystalline diffraction area and the total area of the diffraction profile. The crystalline diffraction area has been obtained from the total area of the diffraction profile by subtracting the amorphous halo. The amorphous halo has been obtained from the X-ray diffraction profile of an atactic polypropylene sample, then it has been scaled and subtracted to the X-ray diffraction profiles of the samples. The so obtained values of x_c have been then used to evaluate the volume fraction index of crystalline phase ϕ_c given by:

$$\phi_c = \left[\frac{x_c/d_c}{x_c/d_c + (1-x_c)/d_a}\right] \tag{22}$$

with d_c and d_a the mass density of crystalline and amorphous phase. Values of 0.94 and 0.85 g/cm^3 have been assumed for d_c and d_a, respectively, corresponding to the density of crystals of α form of iPP[20] and atactic polypropylene,[21] respectively.

The thermal analysis has been performed with a Mettler-DSC30/2285 apparatus, equipped with a liquid nitrogen cooling system for measurements at low temperature. The scans have been recorded in flowing nitrogen atmosphere at a scan rate of 10 °C/min.

Results and Discussion

Thermal Analysis. The mixing of two different stereoisomers of vinyl polymers to obtain new materials with improved properties is not uncommon.[3,22] In the case of polypropylene, the studies performed to date have delineated the neat difficulties encountered at direct probing the level of miscibility of the different stereoisomers in the melt and building the phase diagram of the corresponding blends.[22] This is due to the similar refractive index of the two components in the melt and the scarce effect of the degree of stereoregularity on the glass transition temperature T_g, which is around 0 °C regardless of type (isotactic, syndiotactic or atactic) and degree of stereoregularity.[23] In addition, the study of the thermal behavior of these blends by standard DSC measurements, is complicated by the fact that the melting point depression of a semicrystalline polymer blended with another component is generally very small.[1a,2,24] As argued by Mandelkern,[24] this is an intrinsic properties of polymer blends since the melting point depression is a colligative property and the added species are generally of high molecular mass. The blends used in this paper are a typical example of this category of mixtures.

Representative DSC thermograms recorded during heating and successive cooling of melt pressed films of iPP1/iPP2 blends and pure components are shown in Figure 2, whereas in Figure 3 their thermal behavior is summarized.

The melting and crystallizzation DSC curves of our blends (curves b−d of Figure 2) show, regardless of composition, well separated peaks at temperatures close to those of pure components. In particular at high temperature a single melting and crystallization peak (curves b−d of Figure 2) is present at ≈154 and ≈112 °C respectively, close to the temperatures of corresponding melting and crystallization peaks of the highly stereoregular iPP1 sample (curve a of Figure 2), respectively. At low temperatures, the double melting transition of the low stereoregular iPP2 sample in the range 50−90 °C (curve e of Figure 2A) is retained in the blends (curves b−d of Figure 2A), whereas the low temperature crystallization peaks in the blends

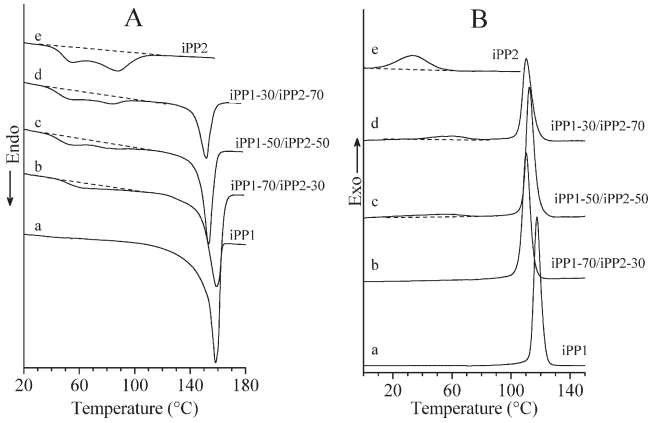

Figure 2. DSC heating (A) and cooling (B) scans, recorded at 10 °C/min, of compression molded samples of the iPP1/iPP2 blends of the indicated composition (b−d) and pure components (a, e).

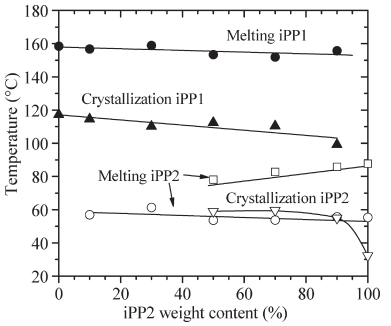

Figure 3. Values of melting and crystallization temperatures of melt pressed samples of iPP1/iPP2 blends and neat components.

occurs at 55−60 °C (curves b-d of Figure 2B) and is located at temperatures ≈30 °C higher than the crystallization temperature of neat iPP2 equal to 32 °C (curves e of Figure 2B).

The thermal behavior of our blends is typical of blends from semicrystalline/semicrystalline polymers with components showing separate and sequential crystallization and melting, one component crystallizing and melting at high temperatures and the second component crystallizing and melting at lower temperatures, with scarce tendency to form crystalline molecular complexes. In particular, in the case of iPP1/iPP2 blends, as shown in Figure 3, the melting temperature of iPP1 and iPP2 components and the crystallization temperature of iPP1 decrease only slightly with increasing the concentration of the second component, and only the crystallization temperature of iPP2 undergoes remarkable increase upon blending.

The DSC data of Figure 2 with the melting point depression could suggest that the crystallization of iPP1 and iPP2 in the blends takes place from a homogeneous melt, where the two components are mixed at molecular level, rather than from a phase separated melt due to a liquid−liquid phase separation before crystallizzation. In particular, the melting point depression of both components in the blends may be attributed to thermodynamic effects, due to the lowered chemical potentials of the chains in the blends as compared to those of neat components,[2,3,24] coupled to the smaller lamellar thickness achieved by crystals in presence of a second component (morphological effect).[3] The fact that this melting depression is quite low, could indicate that owing to the chemical similarity of the two components, the reciprocal interactions are so weak, that the chemical potentials are not greatly affected. This also indicates that the lamellar thickness achieved by iPP1 and iPP2 upon crystallization in the

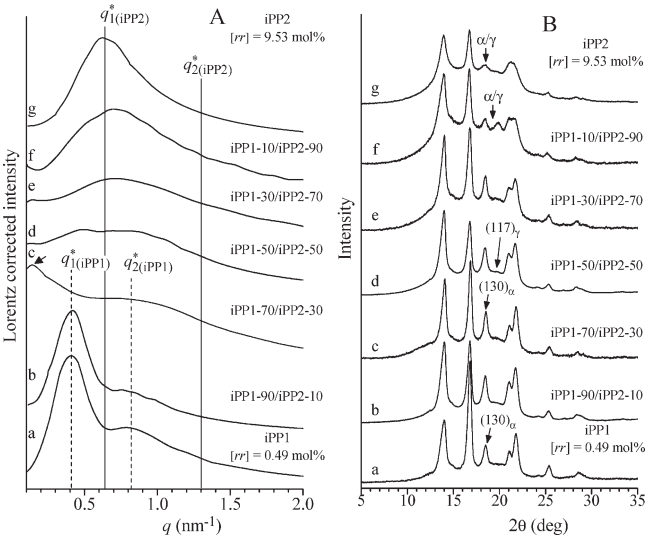

Figure 4. Lorentz-corrected SAXS intensities (A) and corresponding WAXS profiles (B) of as prepared compression molded samples of iPP1 (a), iPP2 (g), and the iPP1/iPP2 blends (b−f) with the indicated compositions. The SAXS profiles in A have been normalized by the corresponding scattering invariant defined by eq 21. The data have been collected at room temperature. Arrow in A for curve c points at a faint maximum at $q \approx 0.14$ nm^{-1} for the blend iPP1−70/iPP2−30 with 70 wt % iPP1.

blends should be similar to those of pure components, crystallized in similar conditions.

On the other hand, the small decrease of crystallization temperature of the high temperature crystallizing (HTC) component iPP1 in the blends probably reflects a slowing down of crystallization kinetics essentially due to dilution effect.[2,3] In fact, since the glass transition temperatures of iPP1 and iPP2 are similar (around 0 °C),[14] we do not expect gross kinetics and morphological variations due to this effect. Finally, the remarkable increase of crystallization temperature by ≈30 °C of the low temperature crystallizing (LTC) component (iPP2) with respect to the crystallization temperature of pure iPP2 (Figure 3) may be attributed to the fact that since its crystallization takes place only after crystallization of the HTC component (Figure 2B), the presence of already formed crystals of iPP1 produces a nucleation effect.

Structural Analysis. As evidenced by DSC analysis, iPP1 and iPP2 components do not lose their ability to crystallize upon blending forming independent lamellae with scarce or no tendency to form cocrystals. In this section we analyze the structural organization of the melt pressed films of our blends at nanometer length scale using standard SAXS measurements, without subjecting the samples to any thermal or chemical treatment aimed at improving the lamellar morphology which develops in non controlled crystallization conditions. Our aim is to boost the use of conventional SAXS measurements with intensity in a relative scale and of conventional methods for analysis of data, for extracting quantitative information related to the lamellar morphology which develops in samples crystallized far from ideal conditions as generally obtained in industrial processes.

In Figure 4, the SAXS and WAXS profiles of as prepared compression molded films of pure components and blends are reported. The SAXS intensity reported in Figure 4A have been multiplied by the Lorentz factor after background subtraction and desmearing (see Experimental Section) and then normalized at having equal area.

The number and kinds of phases present in our samples have been analyzed using the WAXS data of Figure 4B. These data indicate that all iPP1/iPP2 blends are crystallized in the α or

Table 2. Values of the Peak Position (q^*) and Width at Half-Height (W) in the Lorentz Corrected SAXS Profiles of Figure 4A, Average Long Spacing $\langle L_B \rangle$, Average Thickness of Crystalline $\langle l_{cB} \rangle$ and Amorphous Layers $\langle l_{aB} \rangle$, Volume Fraction Index of Crystalline Phase (ϕ_c), Specific Inner Surface (S/V), Correlation Length (l_p), and Deviation Parameter from the Ideal Lamellar Structure ($1/2\langle L_B \rangle S/V$) of As-Prepared Compression Molded Films of Neat iPP1 and iPP2 Samples and iPP1/iPP2 Blends

sample	q^* (nm^{-1})	W (nm^{-1})	$\langle L_B \rangle^a$ (nm)	$\langle l_{cB} \rangle^b$ (nm)	$\langle l_{aB} \rangle^c$ (nm)	ϕ_c	S/V (nm^{-1})	$\langle l_p \rangle$ (nm)	$1/2\langle L_B \rangle S/V$
iPP1	0.41	0.25	15.3	10.9	4.4	0.71	0.27	2.5	2.1
iPP1−90/iPP2−10	0.42	0.27	15.0	10.6	4.4	0.71	0.26	1.9	1.9
iPP1−70/iPP2−30						0.65	0.47	1.9	
iPP1−50/iPP2−50	≈0.48; ≈0.82	≈0.96	13.1; 7.7	6.9	6.1	0.53	0.49	2.0	3.2
iPP1−30/iPP2−70	0.71	0.78	8.8	3.7	5.1	0.42	0.50	1.9	
iPP1−10/iPP2−90	0.72	0.76	8.7	3.3	5.4	0.38	0.48	3.2	2.2
iPP2	0.65	0.52	9.7	3.6	6.1	0.36	0.37	3.0	2.1

[a] Estimated as $\langle L_B \rangle \geq 2\pi/q^*$. [b] Obtained as $\langle l_{cB} \rangle = \langle L_B \rangle \phi_c$ [c] Obtained as $\langle l_{aB} \rangle = \langle L_B \rangle - \langle l_{cB} \rangle$.

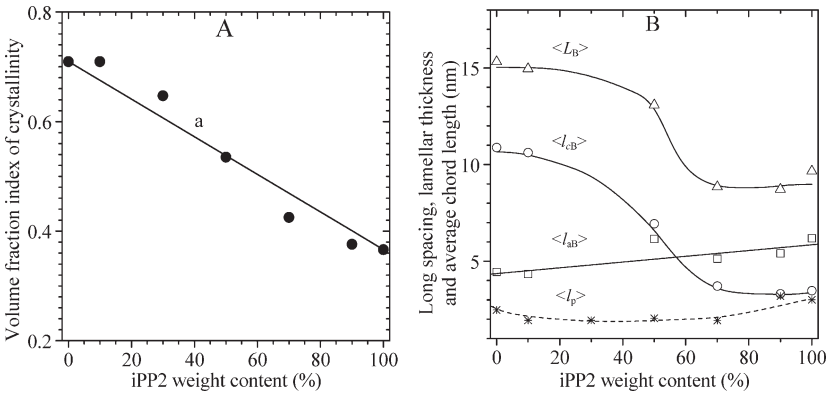

Figure 5. (A) Volume fraction index of crystalline phase of compression molded films of iPP1 and iPP2 samples and iPP1/iPP2 blends as a function of iPP2 concentration (a, ●). B: Average values of long spacing $\langle L_B \rangle$, thickness of crystalline $\langle l_{cB} \rangle$ and amorphous layers $\langle l_{aB} \rangle$, and correlation length $\langle l_p \rangle$ of as prepared compression molded films of iPP1 and iPP2 samples and iPP1/iPP2 blends as a function of iPP2 concentration.

γ forms, or in disordered modifications intermediate between the α and γ forms (α/γ disordered modifications),[25] depending on the composition of the blends. In particular, the highly isotactic sample iPP1 ([*rr*] = 0.49%) and the iPP1/iPP2 blends with iPP1 content higher than 50 wt % are crystallized in the α form (curve a-d of Figure 4B), as indicated by the presence of the $(110)_\alpha$, $(040)_\alpha$ and $(130)_\alpha$ reflections at 2θ = 14, 16.8 and 18.6° of the α form,[20] and the absence of the $(117)_\gamma$ reflection at 2θ = 20.1° of the γ form.[26] The less stereoregular sample iPP2 ([*rr*] = 9.53%) and iPP1/iPP2 blends with iPP1 content lower than 30 wt % crystallize in disordered modification intermediate between α and γ forms,[25] or as mixtures of crystals of α and γ forms, as indicated by the low intensity of $(130)_\alpha$ reflection of α form[20] and/or $(117)_\gamma$ reflection of γ form[26] at 2θ = 18.6 and 20.1° respectively.

It is worth noting that the mass density d_c of crystals of the α[20] and γ[26] forms of iPP is nearly identical, and equal to 0.94 and 0.93 g/cm^3, respectively. Assuming a mass density d_a of ≈0.85 g/cm^3 for the amorphous phase[21] of both iPP1 and iPP2 samples, this indicate that our iPP1/iPP2 blends may be considered as biphasic systems where crystals of the two components of nearly identical mass density and therefore also identical electron density, are embedded in an amorphous matrix of lower density.

The WAXS profiles of Figure 4B have been also utilized to find the volume fraction index of crystalline phase ϕ_c of our samples using eq 22. The values of ϕ_c are collected in Table 2 and are shown in Figure 5A (curve a). The values of ϕ_c decrease almost linearly with increasing the content of the less stereoregular component, from the values achieved by neat iPP1 of ≈0.71 to the value achieved by neat iPP2 of ≈0.36, crystallized in similar conditions, the crystallinity index being only slightly higher than that predicted by the linear relationship in the case of iPP1 rich blends, and only slightly lower in the case of blends rich in the less stereoregular component iPP2. This suggests that the crystallization ability of each of the two components in the iPP1/iPP2 blends is not greatly influenced by the presence of the other component, in agreement with DSC results.

The Lorentz-corrected SAXS intensity distribution of compression molded films of samples iPP1, iPP2 and iPP1/iPP2 blends (curves a, b, e−g of Figure 4A), with the exception of the blends iPP1−70/iPP2−30 and iPP1−50/iPP2−50 (curves c, d of Figure 4A), show in all cases a correlation peak typical of the lamellar morphology. The intensity of correlation peaks in the blends decreases with respect to that of pure components, while a simultaneous increase of the width at half height of the peaks and background intensity all over the sampled q range occurs. The position of maxima (q^*) and width at half height (W) of the main SAXS peaks of Figure 4A are listed in Table 2. In particular the sample iPP1 and the blend iPP90-iPP10 (curves a, b of Figure 4A) show a first and faint second order correlation peak at $q \approx 0.41$ and 0.82 nm^{-1}, respectively. The sample iPP2 shows a single correlation peak at $q \approx 0.65$ nm^{-1} (curve g of Figure 4A), that shifts toward higher q values of ≈0.72 nm^{-1} for the blends iPP10-iPP90 and iPP70-iPP30 (curves e, f of Figure 4A). Finally, the blend iPP1−50/iPP2−50 (curves d of Figure 4A) shows two faint maxima at $q \approx 0.45$ and 0.80 nm^{-1}, whereas for the blend iPP1−70/iPP2−30 (curve c of Figure 4A) no definite maxima are apparent, and only a broad halo centered at $q \approx 0.80$ nm^{-1} with a neat upturn in the low q region is present, faintly peaked around $q \approx 0.14$ nm^{-1} (arrow in Figure 4A, curve c).

From inspection of the Lorentz corrected SAXS profiles of Figure 4A it is apparent that for all melt pressed samples the main correlation peak is broad, even in the case of pure components. In particular, the width at half height of the correlation peak is $W \approx 0.25$ nm^{-1} for neat iPP1, and $W \approx 0.5$ nm^{-1} in the case of neat iPP2, indicating that large deviations from the ideal model of lamellar stacks of Figure 1A,C occur, and namely

that the distribution of thicknesses of amorphous and crystalline layers is quite broad for both components. In the case of blends, the width at half height of the correlation peak gradually increase by addition of the second component. In particular this broadening is small in the case of iPP1 rich blend with 10% iPP2 (iPP1−90/iPP2−10, curve b of Figure 4A), for which the width at half height W increases from $\approx$0.25 nm^{-1} of neat iPP1 to $\approx$0.27 nm^{-1}. In the case of blends rich in iPP2 component, instead the width at half height of the main correlation peak W increases from $\approx$0.50 nm^{-1} of neat iPP2 (curves g of Figure 4A) to $\approx$0.75−0.80 nm^{-1} for blends iPP1−10/iPP2−90 and iPP1−30/iPP2−70, with 10 and 30 wt % iPP1 (curves e, f of Figure 4A). Finally in the case of blends iPP1−50/iPP2−50 with equal weight fraction of the two components, a single ill defined double peaked hump with $W \approx 1$ nm^{-1} is observed (curve d of Figure 4A) whereas for the blend iPP1−70/iPP2−30 with 30 wt % iPP2 no well-defined correlation peak is present, and only diffuse scattering occurs (curve c of Figure 4A). The broadening of correlation peaks in the blends, accompanied by the simultaneous increase of diffuse scattering all over the sampled q range, especially in the low q region, could suggest that the lamellar stacks formed in the blends deviate from the ideal model of uniform and regular thickness of crystalline and amorphous layers of Figure 1A, C, not only because the distribution of these thicknesses are broad as in the case of pure components, but also because additional disorder is present.

The remarkable changes of SAXS intensity distribution shown by iPP1/iPP2 blends as a function of composition and in particular the increase of the width at half height of correlation peaks and of background intensity observed in the SAXS profiles from iPP1/iPP2 blends, up to achieve a nearly featureless SAXS intensity distribution from blends with iPP2 content in the range 30−50 wt % (curves c-d of Figure 4A), could suggest random mixing between the lamellae of iPP1 and iPP2 components in the blends, rather than formation of separated lamellar stacks from the two components. In fact, in the latter case, the scattered intensity from different blocks arising from the presence of segregated arrangements of lamellae from the two components would contribute additively to the total intensity, giving rise to two well separated peaks or well recognizable shoulders, without producing any effect on the background intensity all over the sampled q range. Only in the case that the average size of lamellar stacks D would be of the same order as the average interlamellar spacing (long spacing), or no lamellar stacks at all were formed, a large background could affect our SAXS data in the relevant q range.

From the peak position, q^*, the average value of long period $\langle L_B \rangle$ can be obtained as $\langle L_B \rangle \approx 2\pi/q^*$ (where subscript B indicates that we have applied the Bragg law for evaluation of this parameter). It is apparent that the value of $\langle L_B \rangle$ is $\approx$15 nm for neat iPP1 and iPP1/iPP2 blend with iPP2 content of 10 wt %, is $\approx$9.7 nm in the case of iPP2 and decreases to $\approx$9 for iPP1/iPP2 blends with iPP2 content of 90 and 70%. Since in our blends both components are semicrystalline the measured values of long period of blends may be assumed to be the average interlamellar spacing between iPP1 and iPP2 lamellae.

The values of $\langle L_B \rangle$, in turn, can be used for a rough evaluation of the average thicknesses of crystalline and amorphous layers $\langle l_{cB} \rangle$ and $\langle l_{aB} \rangle$, respectively given by $\langle l_{cB} \rangle \approx \langle L_B \rangle \phi_c$ and $\langle l_{aB} \rangle \approx \langle L_B \rangle - \langle l_{cB} \rangle$. The values of $\langle L_B \rangle$, $\langle l_{cB} \rangle$, and $\langle l_{aB} \rangle$ are reported in Table 2 and are shown in Figure 5B as a function of blend composition. It is apparent that the average thickness of amorphous phase in between the crystalline lamellae $\langle l_{aB} \rangle$ increases almost linearly with iPP2 concentration in the blends from the value of 4.4 nm of neat iPP1 to the value of 6.1 of neat iPP2. The average values of lamellar thickness $\langle l_{cB} \rangle$ instead closely mimic those of interlamellar spacing $\langle L_B \rangle$ and are $\approx$11 nm for neat iPP1 and iPP1 rich blends and $\approx$3.5 nm for neat iPP2 and iPP2 rich blends. The largest deviations from these trends occur for blends with iPP1 concentration in the range 30−50 wt %, for which the position of maxima is ill-defined. Average values of long spacing, lamellar thickness and thickness of amorphous layers of iPP1, iPP2, and iPP1/iPP2 blends (with the exception of the blends with iPP2 content 30−50 wt %) may be obtained also resorting to the classic method based on the evaluation of autocorrelation function of electron density fluctuations normalized by the scattering invariant,[6] and indeed the values of these parameters evaluated with this method are very similar to those calculated directly from Lorentz corrected SAXS curves, plotted in Figure 4A. Since this kind of analysis would not add any new information, these data are not shown. Indeed, the most important result of analysis of Figure 4A consists in the fact the in iPP1 rich blends and in iPP2 rich blends the average values of morphological parameters which characterize the lamellar stacking are dominated by the major component, whose lamellar thickness is not significantly perturbed by the presence of the minor component.

We have also checked the nature of interface between amorphous and crystalline regions. As illustrated in the Experimental Section, indeed, the SAXS desmeared curves after subtraction of the residual background intensity (approximated as a constant) has been extrapolated to high q values with the aid of the Porod law,[18] in the hypothesis that no diffuse boundary between crystalline and amorphous layers occur, by fitting the experimental data in the high q region ($1.5 \text{ nm}^{-1} < q < 3 \text{ nm}^{-1}$) with eq 20. The results of this fit are shown in Figure 6. Of course, transition zones at the lamellar surfaces are expected to lead to deviations from Porod law. The good fitting of the tails of desmeared SAXS profiles from iPP1, iPP2 and iPP1/iPP2 blends to the Porod law even at $q < 1.5$ nm^{-1} indicates that the boundary between the amorphous and crystalline layers may be considered sharp, with no diffuse interface.[18]

As a further check, we have also evaluated the specific inner surface S/V of the as prepared compression molded films of our samples with the aim of determining the length scale of heterogeneity which characterize their structure[18] and to gain indirect information relative to the degree of deviation of the structure from the ideal lamellar model.[6c] To this aim, since our systems may be considered to a good approximation as a random dispersion of two phases (crystalline and amorphous regions) of volume fractions ϕ_c and $(1 - \phi_c)$ and definite composition, the values of the constant K_p obtained by the fits of Figure 6 with the Porod law (eq 20), and the scattering invariant Q evaluated through eq 21 have been used to find the specific inner surface of our systems S/V, using

$$\frac{S}{V} = \frac{K_p}{2\pi Q}\phi_c(1-\phi_c) \tag{23}$$

The inverse of specific inner surface has the dimension of a length and is as a measure of the length scale of heterogeneities (crystalline and amorphous regions) that characterizes the structure of our blends $\langle l_p \rangle$. This parameter is given by:

$$\langle l_p \rangle = \frac{4\phi_c(1-\phi_c)}{S/V} = \frac{8\pi Q}{K_p} \tag{24}$$

The values of S/V and $\langle l_p \rangle$ of our samples are listed in Table 2, and those of $\langle l_p \rangle$ are also reported in Figure 5B . In practice, the value of $\langle l_p \rangle$ may be considered as a measure of the average size of the heterogeneities present in a system. These values are in all cases comprised between 2 and 3 nm in our systems indicating that the length scale of heterogeneities which characterize the structure of pure components is not greatly modified upon blending.

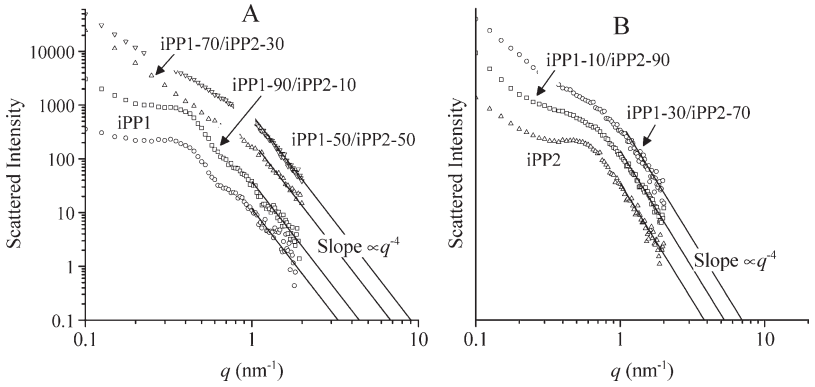

Figure 6. Desmeared SAXS intensity distribution of as prepared compression molded films of iPP1 (A, ○) and iPP2 (B, Δ) neat samples and iPP1/iPP2 blends with 10 (A, □), 30 (A, Δ), 50 (A, ▽), 70 (B, ○) and 90 wt % (B, □) iPP2. The experimental data for $q > 2$ nm^{-1} have been cut, to better visualize the q^{-4} scaling of the tail region.

Finally, the halved product of the average long spacing $\langle L_B \rangle$ and specific inner surface area S/V, i.e. $1/2\langle L_B \rangle S/V$, has been used as a disorder parameter which characterizes the deviations of the structure of our samples from the ideal lamellar model.[6c] The value of this product should be 1 for the ideal lamellar model.[6c] The values of the disorder parameter of our systems are reported in Table 2. It is apparent that it is around 2 in all cases with the exception of the blend iPP1−50/iPP2−50, for which this product is close to 3. Such large positive deviations from unity are only in part due to the large error associated with the approximated evaluation of the average long spacing $\langle L_B \rangle$, but rather indicate that a large amount of disorder is present in our systems, due to formation of curved lamellae, presence of amorphous regions outside the lamellar stacks, voids and other heterogeneities of the same size as the lamellar thickness. However, whatever the origin of such disorder, the most important result is that such defects are already present in the neat iPP1 and iPP2 components, and may not be responsible for the remarkable changes observed in the SAXS intensity distribution (Figure 4A and 6) of blends.

In conclusion, the results of the analysis performed in this section strongly support the hypothesis that the mixing of the two samples of iPP with different degree of stereoregularity gives rise to mixtures which are miscible in the melt, where the two components tend to crystallize forming mixed lamellar stacks. The thickness of amorphous and crystalline layers and layer thickness distribution of neat components is not largely affected in the blends, and the so obtained structures may be confidently modeled as nearly biphasic systems with sharp boundary between the amorphous and crystalline layers, completely neglecting the presence of diffuse interfaces.

X-ray Modeling. We have used eq 14 derived in the Modeling section to calculated one-dimensional SAXS profiles from ideal models of lamellar structures including stacking fault disorder to be compared with the experimental Lorentz-corrected SAXS profiles of our samples shown in Figure 4A. Such disorder consists of lamellar crystals of different thickness stacked with faults along the z directions (Figure 1B) according to different statistical models, ranging from completely random, to more block configurations. For the sake of simplicity, the calculations are shown only for the two limiting statistics, the completely random model, and the block configuration. We recall that in the latter case the two kind of layers form separated stacks and the scattering intensity from different blocks contribute additively to the total scattering intensity.

We have assumed that two kinds of lamellae are mixed, fixing the ratio of the lamellar thickness l_{cm} to the long period L_m of each kind of lamellae equal to $l_{c1}/L_1 = 0.71$ for the lamellae of kind 1 and $l_{c2}/L_2 = 0.36$ for the lamellae of kind 2.

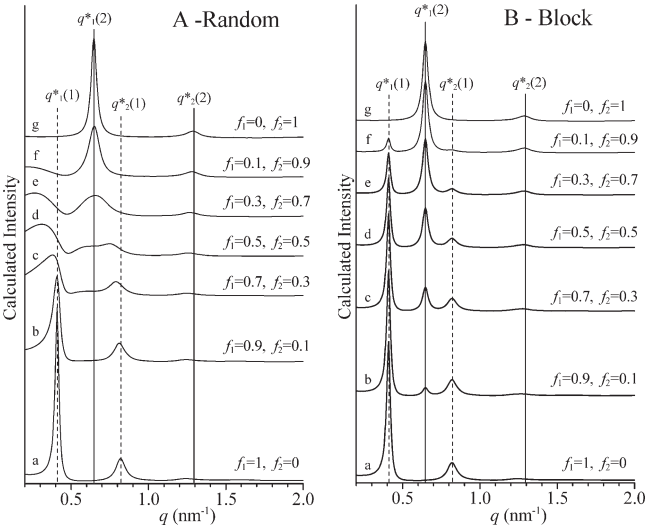

Figure 7. Calculated one-dimensional SAXS profiles for the statistical model with random (A) and block (B) configuration, and the indicated degree of inclusion of the two kind of layers in the stack, with $f_1 = 1, f_2 = 0$ corresponding to pure component 1 (a), $f_1 = 0, f_2 = 1$ corresponding to pure component 2. Calculations have been performed by setting the values of relative standard deviations of the distribution of thickness of amorphous and crystalline layers $\sigma/l_{c1} = \sigma/l_{a1} = \sigma/l_{c2} = \sigma/l_{a2} = 0.1$, long spacing, and thickness of amorphous and crystalline layers $L_1 = 15.3$ nm, $l_{c1} = 10.9$ nm, $l_{a1} = 4.9$ nm for the component 1, and $L_2 = 9.7$ nm, $l_{c2} = 3.6$ nm, $l_{a2} = 6.1$ nm for the component 2, respectively, and average number of crystalline lamellae in the stack $\langle N \rangle = 10$. The position of first $q_1(m)$ and second order $q_2(m)$ ($m = 1, 2$) peaks from stacks of pure components 1 and 2 are indicated by vertical lines.

The value of l_{cm}/L_m corresponds to the so-called linear degree of crystallinity, and is generally close to the volume fraction index of crystallinity determined with a different technique. In our case the values of 0.71 and 0.36 correspond to the volume fraction index of crystallinity ϕ_c of as prepared compression molded films of neat iPP1 and iPP2 samples (see Table 2). In view of the nearly identical electron density from crystals of iPP1 and iPP2, and that also the electron density of amorphous phase of neat components may be assumed identical, the value of contrast $\Delta\rho_m$ of species 1 and 2 has been considered identical in eq 15, so that the exact value of this parameter does not affect the calculations.

In Figure 7, the calculated SAXS profiles are shown for different degree of inclusion of the two kind of lamellae in the stack, ranging from pure component 1 (i.e., $f_1 = 1, f_2 = 0$), to pure component 2 (i.e., $f_1 = 0, f_2 = 1$), for the statistical random model (A) and the block configuration (B).

In these calculations the relative standard deviations of the distribution of thickness of amorphous and crystalline layers σ/l_{cm} and σ/l_{am}, respectively, has been fixed equal to 0.1 for both the components. The values of the long spacing L_1 and L_2 have been assumed identical to those of neat iPP1 and iPP2 components in the as prepared compression molded films and equal to 15.3 and 9.7 nm respectively, so that also the values of thickness of crystalline l_{cm} and amorphous layers l_{am} coincide with the experimental values shown by neat iPP1 and iPP2, corresponding to $l_{c1} = 10.9$ nm, $l_{a1} = 4.9$ nm for the component 1, and $l_{c2} = 3.6$ nm, $l_{a2} = 6.1$ nm for the component 2, respectively (see Table 2). Finally, finite dimensions of the lamellar stacks along z have been assumed with a Bernoulli type distribution, by setting the average number of crystalline lamellae in the stack $\langle N \rangle = 10$.

The calculated profiles of Figure 7 from stacks of pure systems 1 and 2 (curves a, g of Figure 7) show narrow peaks at the same positions of first and second order correlation peaks observed in the case of as prepared compression molded films of neat iPP1 and iPP2 samples (curves a, g of Figure 4A), i.e. $q_1(1) \approx 0.41$ nm^{-1}, $q_2(1) \approx 0.82$ nm^{-1}, for the pure system 1, $q_1(2) \approx 0.65$ nm^{-1}, $q_2(1) \approx 1.3$ nm^{-1}, for the pure system 2. Although the width at half height of these peaks is much narrower than the experimental one, (due to the small value of relative standard deviation for the thickness of crystalline and amorphous layers assumed in the calculations), the calculated profiles for the mixed systems show some interesting features. In fact, apart from the trivial result obtained in the case of the block configuration (Figure 7B) for which the profiles of pure systems 1 and 2 contribute additively to the total scattering intensity distribution in the mixed systems (curves b−f of Figure 7B), the calculated profiles obtained for the randomly mixed lamellar stacks (curves b−f of Figure 7A) show that increasing the degree of inclusion of lamellae of kind 2 within the stack of lamellae 1 (curves b, c of Figure 7A), and of lamellae of kind 1 within the stack of lamellae 2 (curves e, f of Figure 7A) the correlation peaks become broader and broader and tend to shift toward lower q positions. When the degree of inclusion of lamellae from the two components within the stacks becomes identical (i.e., $f_1 = f_2 = 0.5$), the first order peak of the pure system 2 at $q_1(2) \approx 0.65$ nm^{-1} and the second order peak of pure system 1 at $q_2(1) \approx 0.82$ nm^{-1} merge into a single broad peak, spanning the region 0.5−1 nm^{-1} (curves d of Figure 7A). Simultaneously a large increase of diffuse scattering subtending the correlation peaks occurs, especially in the low q tail range. One of the drawback of this kind of calculation is that a zero order peak is always calculated nonzero,[6] whereas in the experimental Lorentz corrected curves the zero-order peak is zeroed due to multiplication by q^2. Actually, the width at half height of the zero-order peak increases with decreasing the dimension of the stack along z, and with increasing the standard deviation and the degree of disorder.

More realistic calculated diffraction profiles with broader peaks, showing width at half-height close to those normally observed in the case of samples crystallized in isothermal conditions at high temperatures ($\approx$0.2 nm^{-1}) could be obtained by increasing the value of the relative standard deviation of the distribution of thickness of amorphous and crystalline stacks to values close to 0.3. As an example, in Figure 8 we show the calculated SAXS profiles obtained by setting $\sigma/l_{c1} = \sigma/l_{a1} = \sigma/l_{c2} = \sigma/l_{a2} = 0.3$. Such broadening corresponds itself to a shift of correlation peak in the calculated patterns toward lower values of q. In order to keep the position of these peaks for pure components 1 and 2 close to those observed in the case of neat iPP1 and iPP2 the values of long spacing L_1 and L_2 have been slightly reduced, while keeping the ratio $l_{c1}/L_1 \approx 0.71$ and $l_{c2}/L_2 \approx 0.36$, by setting $L_1 = 14.3$ nm, $l_{c1} = 10.15$ nm, $l_{a1} = 4.15$ nm for the component 1, and $L_2 = 9.3$ nm, $l_{c2} = 3.35$ nm, $l_{a2} = 5.95$ nm for the component 2. Since for large values of the parameter σ the calculated profiles are not very sensitive to the dimensions along z of lamellar stacks provided that the average number of crystalline layers in the stacks $\langle N \rangle$ is higher than 3, the calculations of Figure 8 correspond to the limit of stacks of infinite length ($\gamma = 0$ in eq 12). Also in this case the calculations have been performed for the two limit statistical models of disorder in the succession of lamellar crystals in the stack, the random configuration (Figure 8A) and the block one (Figure 8B).

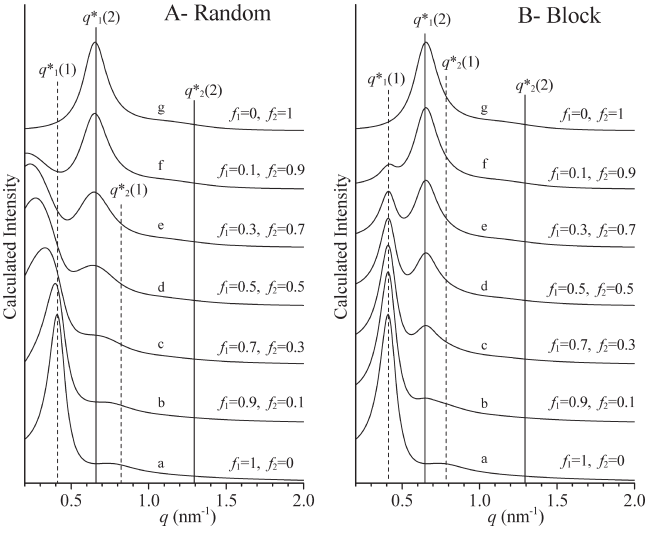

Figure 8. Calculated one-dimensional SAXS profiles for the statistical model with random (A) and block (B) configuration, and the indicated degree of inclusion of the two kind of layers in the stack, with $f_1 = 1, f_2 = 0$ corresponding to pure component 1 (a), $f_1 = 0, f_2 = 1$ corresponding to pure component 2. Calculations have been performed by setting the values of relative standard deviations of the distribution of thickness of amorphous and crystalline layers $\sigma/l_{c1} = \sigma/l_{a1} = \sigma/l_{c2} = \sigma/l_{a2} = 0.3$, long spacing, and thickness of amorphous and crystalline layers $L_1 = 14.3$ nm, $l_{c1} = 10.15$ nm, $l_{a1} = 4.15$ nm for the component 1, and $L_2 = 9.3$ nm, $l_{c2} = 3.35$ nm, $l_{a2} = 5.95$ nm for the component 2, respectively, in the limit of stacks of infinite length. The position of first $q_1(m)$ and second order $q_2(m)$ ($m = 1, 2$) peaks from stacks of pure components 1 and 2 are indicated by vertical lines.

Although the correlation peaks of the calculated diffraction profiles of Figure 8 remain still too narrow in comparison with the experimental ones, direct comparison of the Lorentz-corrected SAXS curves of Figure 4A with the results obtained with our modeling in Figure 8 allows to gain some important information.

First of all, inspection of profiles of Figure 8B corresponding to the block-like configuration indicate that in no case the changes observed in the experimental SAXS profiles of Figure 4A can be explained simply as the result of additive contribution from lamellar stacks of the two neat components.

Then, confining the attention to the calculated profiles corresponding to the random configuration statistics of Figure 8A, it is apparent that for small random inclusion of lamellar crystals of kind 2 within stacks rich in lamellae of kind 1, up to 10% ($f_1 = 0.9, f_2 = 0.1$, curve b of Figure 8A), only a small broadening of the main correlation peak and a small increase of the background intensity in the low q region is produced. This could explain the changes observed in the SAXS profiles of Figure 4A, in going from neat iPP1, to the blend iPP1−90/iPP2−10, with 10 wt % iPP2 (curves a,b of Figure 4A). The profile of blend iPP1−90/iPP2−10, indeed, is similar to that of neat iPP1, and shows only a slight broadening of the correlation peak, and a slight increase of the background intensity. This suggests that iPP2 lamellar crystals formed in this blend are almost totally included in the lamellar stacks of iPP1 component.

In the case of calculated profiles of Figure 8A, remarkable changes occur already for the random inclusion of ≈30% lamellae of kind 2 within the stacks of lamellae of kind 1 ($f_1 = 0.7, f_2 = 0.3$, curve c of Figure 8A). The calculated profile, indeed, shows just a small hump at $q \approx 0.7$ nm^{-1}, a neat upturn in the low q region and large amount of diffuse scattering all over the spectrum. A similar profile is obtained in the case of random inclusion of ≈50% lamellae of kind 2 within the stacks of lamellae of kind 1 ($f_1 = 0.5, f_2 = 0.5$, curve d of Figure 8A), the major differences with curve c consisting in the presence of a more pronounced hump at $q \approx 0.65$ nm^{-1}, a less pronounced upturn in the low q region and larger amount of diffuse scattering all over the spectrum. The calculated profiles of kind c, d of Figure 8A are in qualitative agreement with the nearly featureless SAXS curve of blend iPP1−70/iPP2−30, containing 30 wt % iPP2 (curve c of Figure 4A). Probably, at this composition the maximum degree of inclusion of iPP2 lamellae within the lamellar stacks of iPP1 component is achieved. On the basis of calculated profiles of Figure 8A, which show that the calculated patterns become nearly featureless already by setting $f_1 = 0.7, f_2 = 0.3$ (curve c of Figure 8A), we argue that the maximum degree of inclusion of iPP2 in the stacks of well formed lamellae of iPP1 component should be around 30%.

The calculated profiles of lamellar stacks rich in the component 2 indicate that the random inclusion of 10% ($f_1 = 0.1$, $f_2 = 0.9$, curve f of Figure 8A) and 30% ($f_1 = 0.3, f_2 = 0.7$, curve e of Figure 8A) lamellae of kind 1 in the stacks of lamellae of kind 2 produces just a neat broadening of the correlation peaks of pure system 2 (curve a of Figure 8A), associated with increase of diffuse scattering at low values of q. In no case these calculated SAXS profiles correspond to those of iPP2 rich blends, with iPP1 content of 10 and 30 wt % (curve f, e of Figure 4A), which show a much higher broadening with respect to neat iPP2. Probably, at these compositions, the experimental SAXS curves reflect the presence of at least two independent family of lamellar stacks. A first family is rich in iPP1 component, which crystallizes at high temperatures, achieving the maximum degree of inclusion of lamellae of iPP2 component. The excess of iPP2 component, which crystallizes at lower temperatures forms the second family of lamellar stacks eventually including the iPP1 lamellae not comprised in the first family. Since the family of lamellar stacks rich in the iPP1 component are highly disordered their contribution to the total intensity consists of large background and broad halos, and only the family of lamellar stacks rich in iPP2 contribute to the maximum, with position close to that of neat iPP2 (curve g of Figure 4A). Formation of two disordered families of lamellar stacks explains also the neat increase of the width at half height W of the main correlation peak observed in the case of blends iPP1−10/iPP2−90 and iPP1−30/iPP1−70, from ≈0.50 nm^{-1} for neat iPP2 to ≈0.75−0.80 nm^{-1} for these blends (curve e,f of Figure 4A and Table 2) as well as the presence of the double-peaked small hump observed in the case of blend iPP1−50/iPP2−50 with 50 wt % iPP2 (curve d of Figure 4A).

Using the information gained from calculations shown in Figure 7 and 8, our theoretical approach has been used to model the experimental SAXS curves of our blends. A direct comparison of experimental (Lorentz corrected) SAXS curves from compression molded films of iPP1 and iPP2 neat components and iPP1/iPP2 blends shown in Figure 4A with calculated profiles is presented in Figure 9. In order to mimic the width of correlation peaks of experimental SAXS curves, in the calculations the values of standard deviations that describe the distribution of thickness of crystalline and amorphous layers have been regulated by setting the values of σ_{ci}/l_{ci} and σ_{ai}/l_{ai} in the range 0.3−0.6. The values of long

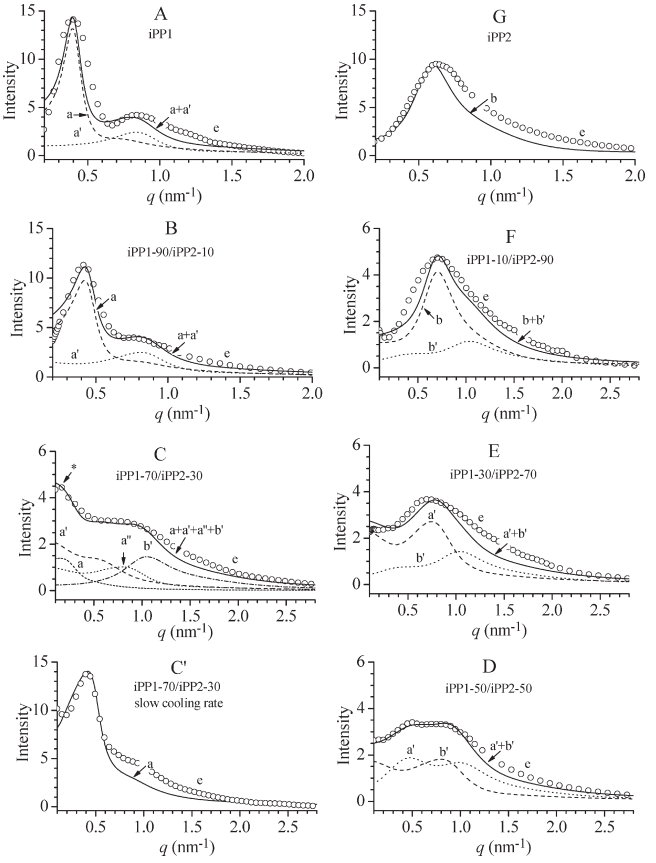

Figure 9. Comparison of slit desmeared SAXS profiles after Lorentz correction from films of iPP1 (A) and iPP2 (G) neat samples, and iPP1/iPP2 blends (B−F, C′) having the indicated composition (e) with the SAXS curves calculated for statistical models with different degree of inclusion of layers from the HTC component 1 defined by $l_{c1}/L_1 = 0.71 \pm 0.10$ and the LTC component 2 defined by $l_{c2}/L_2 = 0.36 \pm 0.10$. Symbols "a" and "b" denote contribution to the SAXS intensity from families of lamellar stacks containing in prevalence the HTC component (a, a′, a″) and the LTC component (b, b′); unprimed symbols are relative to stacks including crystals of the HTC and LTC component with thickness $l_{c1} \approx 10$ nm and $l_{c2} \approx 3$ nm, respectively, primed and double primed symbols are relative to stacks including crystals of the HTC and LTC component with nearly halved thickness, i.e., $l_{c1} \approx 4-5$ nm, $l_{c2} \approx 2$ nm, respectively (see Table 3). The continuous lines correspond to the SAXS curve obtained by summing the various component. Films in parts A−G have been prepared by melt pressing using a flux of cold water within the hot plates during the cooling step; the film in part C′ has been obtained under the same conditions but without using the flux of cold water. The star in part C denotes a faint peak at $q \approx 0.14$ nm^{-1} observed in SAXS curve of iPP1−70-iPP30 blend with 70 wt % iPP1.

spacing L_i, and thicknesses of crystalline and amorphous layers l_{ci} and l_{ai} have been consequently adjusted in order to reproduce the experimental position of correlation peaks. In some cases the presence of more than one family of lamellar stacks could be clearly identified. We have started by simulating the experimental SAXS profiles of the films of neat iPP1 and iPP2 samples. Successively, the SAXS profiles of iPP1/iPP2 blends have been modeled using the morphological parameters found for pure iPP1 and iPP2 to identify the components entering in the various families of lamellar stacks contributing to the total scattered intensity. We address the components entering in each family of lamellar stacks as belonging to the HTC component 1 if the values of L_1/l_{c1} remain high, around 0.71 ± 0.10; as belonging to the LTC component 2 if the values of L_2/l_{c2} are low, around 0.36 ± 0.10. Labels "a" and "b" identify families of lamellar stack containing in prevalence the HTC component 1 and LTC

Table 3. Values of Morphological Parameters Used for Modeling the Slit Desmeared SAXS Profiles after Correction for the Lorentz Factor of Compression Molded Films of Neat iPP1 and iPP2 Samples and iPP1/iPP2 Blends of Figure 9[a]

sample	type of stack	F_{stack}[b]	type of component/stack	l_{ci} (nm)[c]	σ_{ci}/l_{ci}[c]	l_{ai} (nm)[c]	σ_{ai}/l_{ai}[c]	f_i[c]	$\Sigma l_{ci}\,(l_{ci}+l_{ai})^{-1}$	x_c[d]
iPP1	a	0.68	HTC	10.15	0.3	4.15	0.5	1	0.71	0.71
	a′	0.32	HTC	4.61	0.35	1.88	0.5	1		
iPP1−90/iPP2−10	a	0.65	HTC	9.23	0.3	3.77	0.5	0.9	0.67	0.67
			LTC	3.35	0.3	5.59	0.5	0.1		
	a′	0.35	HTC	4.61	0.35	1.88	0.5	0.9	0.67	
			LTC	3.35	0.35	5.95	0.5	0.1		
iPP1−70/iPP2−30	a	0.13	HTC	10.15	0.6	4.15	0.6	0.7	0.61	0.50
			LTC	3.35	0.6	5.95	0.6	0.3		
	a′	0.32	HTC	4.61	0.6	1.88	0.6	0.7	0.61	
			LTC	3.35	0.6	5.95	0.6	0.3		
	a″	0.24	HTC	4.26	0.35	1.74	0.5	0.7	0.61	
			LTC	3.35	0.35	5.95	0.5	0.3		
	b′	0.31	LTC	1.88	0.35	3.35	0.5	1	0.36	
iPP1−70/iPP2−30 slowly cooled	a	1	HTC	8.52	0.3	3.48	0.5	0.7	0.61	0.61
			LTC	3.35	0.3	5.59	0.5	0.3		
iPP1−50/iPP2−50	a′	0.46	HTC	4.26	0.35	1.74	0.5	0.7	0.61	0.49
			LTC	3.35	0.35	5.95	0.5	0.3		
	b′	0.54	LTC	3.35	0.35	5.95	0.5	0.3	0.36	
			LTC	1.88	0.35	3.35	0.5	0.7		
iPP1−30/iPP2−70	a′	0.61	HTC	4.61	0.35	1.88	0.5	0.7	0.61	0.51
			LTC	3.35	0.35	5.95	0.5	0.3		
	b′	0.39	LTC	3.35	0.35	5.95	0.5	0.1	0.36	
			LTC	1.88	0.35	3.35	0.5	0.9		
iPP1−10/iPP2−90	b	0.69	HTC	4.61	0.3	1.88	0.5	0.1	0.40	0.39
			LTC	2.88	0.3	5.12	0.5	0.9		
	b′	0.31	LTC	3.35	0.35	5.95	0.5	0.1	0.36	
			LTC	1.88	0.35	3.35	0.5	0.9		
iPP2	b	1	LTC	3.35	0.3	5.95	0.5	1	0.36	0.36

[a] Labels "a" and "b" identify families of lamellar stack containing a prevailing amount of the high temperature crystallizing (HTC) component 1 and the lower temperature crystallizing (LTC) component 2, respectively; unprimed symbols a, b are relative to stacks including crystals of the HTC and LTC component with thickness $l_{c1} \approx 10$ nm and $l_{c2} \approx 3$ nm, respectively; primed (a′, b′) and double primed (a″) symbols are relative to stacks including crystals of the HTC and LTC component with nearly halved thickness. [b] Fractional amount of the different families of lamellar stack. [c] Thickness of crystalline (l_{ci}) and amorphous layers (l_{ai}), corresponding relative standard deviations (σ_{ci}/l_{ci}, σ_{ai}/l_{ai}) and degree of inclusion (f_i) for the HTC ($i = 1$) and LTC ($i = 2$) components comprised in the families of lamellar stacks of kind "a" and/or "b". [d] Linear degree of crystallinity evaluated as the sum of the partial crystallinity for each family of stacks $\Sigma f_i\, l_{ci}/(l_{ai} + l_{ci})$ multiplied by the corresponding fraction F_{stack}.

component 2, respectively. In Table 3 the characteristic morphological parameters used to simulate the experimental SAXS curves in Figure 9 are collected.

In the case of neat component iPP1, the main features of SAXS distribution intensity (curve e of Figure 9A) could be captured by introducing at least two families of lamellar stacks both characterized by a value of linear crystallinity l_{c1}/L_1 of ≈0.71, coinciding with the experimental value of volume fraction index of crystalline phase. In particular a first family of lamellar stacks of type a consists of well developed crystalline lamellae of average thickness $l_{c1} \approx 10$ nm ($\sigma_{c1}/l_{c1} = 0.3$) separated by amorphous layers of thickness $l_{a1} \approx 4$ nm ($\sigma_1/l_{a1} = 0.5$) (curve a of Figure 9A). A fraction F_{stack} equal to ≈0.68 of these kind of stacks accounts for the main correlation peak at $q \approx 0.40$ nm^{-1} in the experimental profile e. The second family of lamellar stacks, dubbed a′, consists of less perfect crystalline lamellae of nearly halved thickness i.e. with $l_{c1} \approx 5$ nm ($\sigma_{c1}/l_{c1} = 0.35$) separated by amorphous layers of thickness $l_{a1} \approx 2$ nm ($\sigma_1/l_{a1} = 0.5$) (curve a' of Figure 9A). A fraction F_{stack} equal to ≈0.32 of this kind of stacks roughly accounts for the secondary correlation peak at $q \approx 0.80$ nm^{-1} in the experimental profile e.

For the neat component iPP2, the main features of SAXS distribution intensity (curve e of Figure 9G) could be simulated by using a single family of lamellar stacks of kind b characterized by $l_{c2}/L_2 \approx 0.36$ coinciding with the experimental value of volume fraction index of crystalline phase. These stacks consist of crystalline lamellae of average thickness $l_{c2} \approx 3$ nm ($\sigma_{c2}/l_{c2} = 0.3$) separated by amorphous layers of average thickness $l_{a2} \approx 6$ nm ($\sigma_{a2}/l_{a2} = 0.5$) (curve b of Figure 9G).

In the case of iPP1−90/iPP2−10 blend, comprising 90 wt % iPP1, the experimental SAXS distribution intensity (curve e of Figure 9B) is similar to that one of neat iPP1 (curve e of Figure 9A). Accordingly, the main correlation peak at $q \approx 0.40$ nm^{-1} may be accounted for by 65% disordered lamellar stacks of kind a, consisting in the random mixing of 90% HTC component 1 with thickness of crystalline and amorphous layers $l_{c1} \approx 10$ nm ($\sigma_{c1}/l_{c1} = 0.3$) and $l_{a1} \approx 4$ nm ($\sigma_{a1}/l_{a1} = 0.5$) and 10% LTC component 2 with $l_{c2} \approx 3$ nm ($\sigma_{a2}/l_{c2} = 0.3$) and $l_{a2} \approx 6$ nm ($\sigma_{a2}/l_{a2} = 0.5$) (curve a of Figure 9B). The remaining 35% of stacks is reminiscent of the family of kind a′ already present in neat iPP1, and consists of 90% layers from the HTC component 1 with nearly halved thickness of crystals ($l_{c1} \approx 5$ nm − $\sigma_{c1}/l_{c1} = 0.35$, $l_{a1} \approx 2$ nm − $\sigma_{a1}/l_{a1} = 0.5$) randomly mixed with 10% layers from the LTC component 2 ($l_{c2} \approx 3$ nm − $\sigma_{c2}/l_{c2} = 0.35$, $l_{a2} \approx 6$ nm − $\sigma_{a2}/l_{a2} = 0.5$) (curve a′ of Figure 9B). This second fraction of lamellar stacks accounts for the secondary correlation peak at $q \approx 0.80$ nm^{-1} in the experimental profile.

In a similar way, the SAXS profile of iPP2 rich blend, iPP1−10/iPP2−90, comprising only 10 wt % iPP1, (curve e of Figure 9F) is close to that one of neat iPP2 (curve e of Figure 9G). The main correlation peak at $q \approx 0.70$ nm^{-1}, indeed, may be accounted for by a disordered lamellar stack of kind b comprising 90% layers from LTC component 2 with $l_{c2} \approx 3$ nm ($\sigma_{c2}/l_{c2} = 0.3$) and $l_{a2} \approx 6$ nm ($\sigma_{a2}/l_{a2} = 0.5$), randomly mixed with 10% defective layers of HTC component 1 with $l_{c1} \approx 5$ nm ($\sigma_{c1}/l_{c1} = 0.3$) and $l_{a1} \approx 2$ nm ($\sigma_{a1}/l_{a2} = 0.5$) (curve b of Figure 9F). In order to account for the presence of the long tail region for $q > 1$ nm^{-1} in the experimental curve e, a second family of lamellar stacks of kind b′ had to be introduced, including exclusively layers of the LTC component 2 (i.e., with $l_c/L \approx 0.36$), where 10% of layers with $l_{c2} \approx 3$ nm − $\sigma_{c2}/l_{c2} = 0.35$, $l_{a2} \approx 6$ nm − $\sigma_{a2}/l_{a2} = 0.5$, characteristics of neat iPP2

sample (Figure 9G), are randomly mixed with 90% layers comprising crystals of nearly halved thickness ($l_{c2'} \approx 2$ nm $- \sigma_{c2}/l_{c2} = 0.35$, $l_{a2'} \approx 3$ nm $- \sigma_{a2'}/l_{a2'} = 0.5$) (curve b′ of Figure 9F). The relative amount of stacks of kind b and b′ is 69% and 31%, respectively (see Table 3). No detectable amount of lamellar stacks including well-formed lamellar crystals of the HTC component with $l_{c1} \approx 10$ nm could be detected, either because the correlation peak from these stacks occurs at q less than our resolution limit ($q_{min,} \approx 0.1$ nm^{-1}) and their amount is very low or because these crystals are not formed at all when the concentration of iPP1 component is below a threshold limit.

Having identified the leading families of lamellar stacks formed in our system, the modeling of SAXS profiles of iPP1−70/iPP2−30, iPP1−50/iPP2−50 and iPP1−30/iPP2−70 blends comprising 70, 50, and 30 wt % iPP1 (curve e of Figure 9C−E) is straightforward. We first notice that in all three cases the SAXS profiles of Figure 9C−E feature a long tail region for $q > 1$ nm^{-1} as in the case of blend iPP1−10/iPP2−90 (Figure 9F). This indicates that in these blends a portion of stacks of kind b′ is present, including lamellae of the LTC component 2 of low thickness. The reason why lamellar stacks of kind b′ containing crystals of iPP2 component of low thickness are apparent in the blends with iPP1 concentration in range 10−70 wt % and not in the neat iPP2 sample may be envisaged in the fact that in presence of the more stereoregular iPP1 component, a sort of fractionation occurs. Only the most stereoregular portions of chains of iPP2 component are included in the stacks in between the crystalline lamellae of iPP1 component which form at high crystallization temperatures, so that the less stereoregular portions of iPP2 chains are rejected in the interlamellar regions and form disordered stacks, where irregular crystals of small thickness of the LTC component 2 are embedded.

In particular, the SAXS profiles of blends iPP1−50/iPP2−50 and iPP1−30/iPP2−70 (curve e of Figure 9D, E) may be described in terms of at least two contributions. More precisely, for the blend iPP1−50/iPP2−50 the experimental double peaked SAXS profile of Figure 9D (curve e) may be accounted for by the presence of stacks of kind a′ arising from the random mixing of 70% layers of HTC component 1 with thickness $l_{c1} \approx 4$ nm ($\sigma_{c1}/l_{c1} = 0.35$), $l_{a1} \approx 2$ nm ($\sigma_{a1}/l_{a1} = 0.5$) and 30% layers of the LTC component 2 with $l_{c2} \approx 3$ nm ($\sigma_{c1}/l_{c1} = 0.35$), $l_{a2} \approx 6$ nm ($\sigma_{a1}/l_{a1} = 0.5$) (curve a′ of Figure 9D), whereas the long tail region is accounted for by the presence of stacks of kind b′ including 30% layers from the LTC component 2 with $l_{c2} \approx 3$ nm $- \sigma_{c2}/l_{c2} = 0.35$, $l_{a2} \approx 6$ nm $- \sigma_{a2}/l_{a2} = 0.5$, randomly mixed with 70% layers still of LTC component 2, but with crystals of nearly halved thickness (i.e., $l_{c2'} \approx 2$ nm $- \sigma_{c2}/l_{c2} = 0.35$, $l_{a2} \approx 3$ nm $- \sigma_{a2}/l_{a2} = 0.5$) (curve b′ of Figure 9D), the relative amount of stacks of a′ and b′ being ≈50% (see Table 3). For the blend iPP1−30/iPP2−70, instead, the primary correlation peak at $q \approx 0.80$ nm^{-1} of experimental SAXS profile of Figure 9E (curve e) may be accounted for by the presence of stacks of kind a′ arising from the random mixing of 70% layers of HTC component 1 with thickness $l_{c1} \approx 5$ nm ($\sigma_{c1}/l_{c1} = 0.35$), $l_{a1} \approx 2$ nm ($\sigma_{a1}/l_{a1} = 0.5$) and 30% layers of the LTC component 2 with $l_{c2} \approx 3$ nm ($\sigma_{c1}/l_{c1} = 0.35$), $l_{a2} \approx 6$ nm ($\sigma_{a1}/l_{a1} = 0.5$) (curve a′ of Figure 9D), whereas the long tail region is accounted for by the presence of stacks of kind b′ including 10% layers from the LTC component 2 with $l_{c2} \approx 3$ nm $- \sigma_{c2}/l_{c2} = 0.35$, $l_{a2} \approx 6$ nm $- \sigma_{a2}/l_{a2} = 0.5$ randomly mixed with 70% layers of LTC component 2 of nearly halved thickness for the crystals ($l_{c2'} \approx 2$ nm $- \sigma_{c2}/l_{c2} = 0.35$, $l_{a2} \approx 3$ nm $- \sigma_{a2}/l_{a2} = 0.5$) (curve b′ of Figure 9F). For this blend, the relative amount of stacks of a′ and b′ is 61% and 39%, respectively (see Table 3). As in the case of blend iPP1−90-iPP2−10 with 90 wt % iPP1, also in the case of blends iPP1−50/iPP2−50 and iPP1−30/iPP2−70 no detectable amount of lamellar stacks including well formed lamellar crystals of the HTC component with $l_{c1} \approx 10$ nm could be detected, probably because the correlation peak from these stacks occurs at q less than our resolution ($q_{min,} \approx 0.1$ nm^{-1}).

Finally, in the case of iPP1−30/iPP2−70 blend with 70 wt % iPP1, the featureless Lorentz corrected SAXS curve from the compression molded film (curve e of Figure 9C) may be described as due to the contribution from more than two families of lamellar stacks. In particular, the high q tail region may be accounted for by a population of lamellar stacks of kind b′ arising from irregular crystals of the LTC component 2 ($l_{c2'} \approx 2$ nm $- \sigma_{c2}/l_{c2} = 0.35$, $l_{a2} \approx 3$ nm $- \sigma_{a2}/l_{a2} = 0.5$) not included in the stacks of the HTC component 1 (curve b′ of Figure 9C). The intensity distribution in the low q region with the upturn and the faint peak at $q \approx 0.14$ nm^{-1} may be accounted for by a family of lamellar stack of kind a, including 70% of well developed crystals of the HTC component 1 with $l_{c1} \approx 10$ nm $- \sigma_{c1}/l_{c1} = 0.6$, $l_{a2} \approx 4$ nm $- \sigma_{a1}/l_{a1} = 0.6$, randomly mixed with 30% layers of the LTC component 2 with $l_{c2'} \approx 3$ nm $- \sigma_{c2}/l_{c2} = 0.6$, $l_{a2} \approx 6$ nm $- \sigma_{a2}/l_{a2} = 0.6$ (curve a of Figure 9C). Lamellar stacks of type a′ and a″ are also present, including 70% layers of the HTC component 1 with crystals of low thickness ($l_{c1} \approx 4-5$ nm, $l_{a1} \approx 2$ nm) randomly mixed with 30% layers of the LTC component 2 with $l_{c2} \approx 3$ nm, $l_{a2} \approx 6$ nm (curves a′ and a″ of Figure 9C). The stacks of kind a′ and a″ account for the experimental SAXS distribution intensity in the q region intermediate between the low q upturn, and high q tail. The fraction of lamellar stacks of kind a, a′, a″, and b′, are 0.13, 0.32, 0.24, and 0.31, respectively. It is worth noting that in the case of compression molded films of iPP1−70/iPP2−30 blend with 70 wt % iPP1, obtained from the melt without using a flux of cold water within the hot plates during the cooling step to room temperature, the slit desmeared SAXS profile, after correction for the Lorentz factor, (curve e of Figure 9C′) may be accounted for by a single family of lamellar stacks of kind a consisting of 70% layers from the HTC component 1 with $l_{c1} \approx 9$ nm $- \sigma_{c1}/l_{c1} = 0.3$, $l_{a2} \approx 3$ nm $- \sigma_{a1}/l_{a1} = 0.5$ randomly mixed with layers from the LTC component 2 with $l_{c2} \approx 3$ nm $- \sigma_{c1}/l_{c1} = 0.3$, $l_{a2} \approx 6$ nm $- \sigma_{a1}/l_{a1} = 0.5$ (curve a of Figure 9C′).

The good agreement of experimental SAXS profiles of our samples with those calculated using our theoretical approach shown in Figure 9, clearly demonstrate the tendency of iPP1 and iPP2 to form mixed lamellar stacks. Formation of mixed lamellar stacks for all blends definitely rules out occurrence of a liquid−liquid phase separation prior crystallization of the HTC component. Crystallization of iPP1, indeed, occurs from a homogeneous melt, at any composition, where the two components are mixed at molecular level. In fact, the formation of mixed lamellar stacks in blends may occur only if the two components are miscible in the melt state.

Formation of mixed lamellar stacks in semicrystalline/semicrystalline blends has been rationalized in terms of the classic parameter δ[1] introduced by Keith and Padden,[27] defined as $\delta = D/G$, where D is the diffusion coefficient of the noncrystallizing component and G the linear growth rate of the crystals. This parameter is a measure of the distance that the noncrystallizing component may diffuse during the time step of crystallization of the first component and must be of the same size of the morphological feature which develops during that time.[1] Only when the value of the parameter δ is less than 1 mixed lamellar stacks may be formed, because a remarkable amount of the low temperature crystallizing component iPP2 remain trapped into the growing lamellar structure of component iPP1. More complex morphologies may also be formed in these conditions, as for instance interpenetrating lamellar stacks of the two components, with only partial inclusion.[1]

Conclusions

A theoretical model has been derived for the calculation of small-angle X-ray scattering (SAXS) from isolated lamellar stacks in which two or more kinds of lamellae are mixed within the same stack according to different statistical models, ranging from the fully random mode, to alternated one, up to block configurations.

We have shown that the SAXS profiles calculated from ideal models of disorder with the judicious choice of the proper parameters may be advantageously compared with the experimental SAXS profiles of polymer blends, obtaining information not easy to gain using different techniques, even in the case of samples crystallized in non controlled conditions.

Our theoretical approach allows overcoming some limitation of more classic methods of analysis of SAXS data, in cases of blends of semicrystalline/semicrystalline polymers crystallized from the melt in conditions far from thermodynamic equilibrium. The classic analysis of SAXS data from these systems, indeed, is complicated by the nearly featureless SAXS profiles obtained for some compositions with no apparent correlation peaks, whereas more direct observations, e.g., with scanning electron microscopy and/or optical microscopy would be highly demanding due to the similar chemical nature of the two components without using some *ad hoc* chemical or thermal treatment.

We have shown that lack of definite correlation peaks in the SAXS profiles associated with the presence of large amount of diffuse scattering shown by some blends does not necessarily correspond to the lack of lamellar morphology, but that these featureless SAXS profiles may also originate from lamellar stacks with the lamellae of the two components randomly mixed within the same array, stacked with faults.

Our modeling approach has been tested in the case of some model blends obtained by mixing two semicrystalline iPP samples characterized by two different melting temperatures. A unified vision of the complex morphology at nanometer length scale of these blends has been obtained, demonstrating that the nanostructural organization of these blends depends on the composition. In all cases, mixed lamellar stacks are formed. In particular, in the case of blends rich in the high temperature crystallizing component iPP1, a high degree of inclusion of lamellae of the second less stereoregular components is achieved, up to reach the maximum degree of inclusion in the blends with 30 wt % iPP2. In the case of blends rich in the less stereoregular component iPP2, at least two families of lamellar stacks are formed, a family rich in iPP1 component, which forms at high temperatures, achieving the maximum degree of inclusion of lamellae of iPP2 component, and a second family which forms at lower temperatures, including the excess of iPP2 component and eventually the iPP1 lamellae not comprised in the first family. Formation of mixed lamellar stacks in these systems provide clear evidence that the two components are miscible in the melt state.

The model derived in this paper is widely more general, and may be easily extended to more complex systems including more than two kinds of lamellae, the presence of transition zones between amorphous and crystalline layers within the stacks, and/or distributions of thickness of amorphous and crystalline layers different from the classic Gaussian one. In view of the large commercial importance that some semicrystalline/semicrystalline blends have achieved, as for instance the blends of differently branched grades of polyethylene, we believe that our kind of approach may help elucidating the complex morphology which develops in these samples, even in the case of manufactures obtained directly from industrial implants, and not necessarily crystallized under controlled conditions.

Acknowledgment. This work was supported by Seven Framework Programme, Project No. 218331 NaPolyNet. Financial support from Basell Poliolefine Italia S.r.l., "a LyondellBasell company" (Ferrara) is gratefully acknowledged.

References and Notes

(1) For two excellent recent reviews on the argument see: (a) Liu, J.; Junnickel, B. J. *J. Polym. Sci., Polym. Phys. Ed.* **2007**, *45*, 1917. (b) Schultz, J. M. *Front. Chem. Chin.* **2010**, *5*, 262.
(2) Groeninckx, G.; Vanneste, M.; Everaert, V. in *Polymer Blends Handbook*, Utracki, L.A. Ed., Kluwer Academic Publishers: Amsterdam, 2003; p 203, Bucknall, P.; Paul, D. R.; Bucknall, C. B. *Polymer Blends*: Wiley-Interscience: New York, 2000.
(3) (a) Nwabunma, D.; Kyu, T. *Polyolefin Blends*; Wiley-Iinterscience: Hoboken, NJ, 2008; (b) Shiomura, T.; Uchikawa, N.; Asanuma, T.; Sugimoto, R.; Fujio, I.; Kimura, S.; Harima, S.; Akiyama, M.; Kohno, M.; Inoue, N. in *Metallocene Based Polyolefins: Preparation, Properties and Technology*; Scheirs, J.; Kaminsky, W., Eds.; Wiley: Chichester, England, 2000; Vol. *1*, pp 437−465.
(4) (a) Khambatta, F. B.; Russell, T.; Warner, F.; Stein, R. S. *J. Polym. Sci., Polym. Phys. Ed.* **1976**, *14*, 1391. (b) Stein, R. S. *Pure Appl. Chem.* **1991**, *41*, 5157. (c) Chen, H. L.; Wang, S. F. *Polymer* **2000**, *41*, 5157. (d) Cheung, Y. W.; Stein, R. S. *Macromolecules* **1994**, *27*, 2512. (e) Cheung, Y. W.; Stein, R. S.; Lin, J. S.; Wignall, G. D. *Macromolecules* **1994**, *27*, 2520.
(5) (a) Runt, J. P.; Zhang, X.; Miley, D. M.; Gallagher, K. P.; Zhang, A. *Macromolecules* **1992**, *25*, 3902–3905. (b) Talibuddin, S.; Wu, L.; Runt, J.; Lin, J. S. *Macromolecules* **1996**, *29*, 7527–7535. (c) Wang, W.; Schultz, J. M.; Hsiao, B. S. *Macromolecules* **1997**, *30*, 4544–4550. (d) Fragiadakis, D.; Dou, S.; Colby, R. H.; Runt, J. *Macromolecules* **2009**, *42*, 6581–6587.
(6) (a) Baltà-Calleja, F. J.; Vonk, C. G. *X-ray Scattering of Synthetic Polymers*: Elsevier: Amsterdam, 1989;(b) Vonk, C. G.; Kortleve, G. *Kolloid-Z. Z. Polymer* **1967**, *220*, 19. (c) Strobl, G. R.; Schneider, M. *J. Polym. Sci.: Polym. Phys Ed.* **1980**, *18*, 1343.
(7) (a) Hendicks, S. B.; Teller, E. *J. Chem. Phys.* **1942**, *10*, 147. (b) Wilson, A. J. C. *Proc. R. Soc. London* **1942**, *180*, 227. (c) Mering, J. *Acta Crystallogr.* **1949**, *2*, 371. (d) Jagodinski, H. *Acta Crystallogr.* **1949**, *2*, 201; Ibidem 208; Ibidem 298;(e) Jagodinski, H. *Acta Crystallogr.* **1954**, *7*, 17. (f) Kakinoki, J.; Komura, Y. *J. Phys. Soc. Jpn.* **1952**, *7*, 30. (g) Kakinoki, J.; Komura, Y. *J. Phys. Soc. Jpn.* **1954**, *9*, 169; Ibidem 177;(h) Kakinoki, J.; Komura, Y. *Acta Crys.* **1962**, *15*, 292.
(8) (a) Allegra, G. *Acta Crystallogr.* **1961**, *14*, 535. (b) Allegra, G. *Nuovo Cim.* **1961**, *21*,786; Ibidem 661;(c) Allegra, G. *Nuovo Cim* **1962**, *23*, 502. (d) Allegra, G. *Acta Crystallogr.* **1964**, *17*, 579.
(9) Allegra, G.; Bassi, I. W. *Gazz. Chim. Ital.* **1980**, *110*, 437.
(10) Resconi, L.; Piemontesi, F.; Camurati, I.; Sudmeijer, O.; Nifant'ev, I. E.; Ivchenko, P. V.; Kuz'mina, L. G. *J. Am. Chem. Soc.* **1998**, *120*, 2308.
(11) Resconi, L.; Balboni, D.; Baruzzi, G.; Fiori, C.; Guidotti, S. *Organometallics* **2000**, *19*, 420.
(12) Nifant'ev, I. E.; Guidotti, S.; Resconi, L.; Laishevtsev, I. (Basell, Italy) *PCT Int. Appl.* WO 01/47939, 2001. Fritze, C.; Resconi, L.; Schulte, J.; Guidotti, S. (Basell, Italy) *PCT Int. Appl.* WO 03/00706, 2003.Resconi, L.; Guidotti, S.; Camurati, I.; Nifant`ev, I. E.; Laishevtsev, I. *Polym. Mater. Sci. Eng.* **2002**, *87*, 76.
(13) Nifant'ev, I. E.; Laishevtsev, I. P.; Ivchenko, P. V.; Kashulin, I. A.; Guidotti, S.; Piemontesi, F.; Camurati, I.; Resconi, L.; Klusener, P. A. A.; Rijsemus, J. J. H.; de Kloe, K. P.; Korndorffer, F. M. *Macromol. Chem. Phys.* **2004**, *205*, 2275. Resconi, L.; Guidotti, S.; Camurati, I.; Frabetti, R.; Focante, F.; Nifant'ev, I. E.; Laishevtsev, I. P. *Macromol. Chem. Phys.* **2005**, *206*, 1405.
(14) De Rosa, C.; Auriemma, F.; Di Capua, A.; Resconi, L.; Guidotti, S.; Camurati, I.; Nifant'ev, I. E.; Laishevtsev, I. P. *J. Am. Chem. Soc.* **2004**, *126*, 17040.
(15) Moraglio, G.; Gianotti, G.; Bonicelli, U. *Eur. Polym. J.* **1973**, *9*, 693.
(16) Bergmann, A.; Orthaber, D.; Scherf, G.; Glatter, O. *J. Appl. Crystallogr.* **2000**, *33*, 869.
(17) Kratky, O.; Stabinger, O. *Colloid Polym. Sci.* **1984**, *262*, 345.
(18) Roe, R.-J. *Methods of X-ray and Neutron Scattering in Polymer Science*; Oxford University Press: New York, 2000;Koberstein, J. T.; Morra, B.; Stein, R. S. *J. Appl. Crystallogr.* **1980**, *13*, 34.
(19) Debye, D.; Beuche, A. M. *J. Appl. Phys.* **1949**, *20*, 518.
(20) Natta, G.; Corradini, P. *Nuovo Cim. Suppl.* **1960**, *15*, 40.
(21) *Polymer Data Handbook*; Mark, J. E., Ed. Oxford University Press: Oxford, U.K., 2009.
(22) Phillips, R. A. *J. Polym. Sci., Part B: Polym. Phys.* **2000**, *38*, 1947. Wang, Z.-G.; Phillips, R. A.; Hsiao, B. S. *J. Polym. Sci., Part B: Polym. Phys.* **2000**, *38*, 2580. Mayer, R.-D.; Thomann, R.; Kressler, J.; Mulhaupt, R.; Bernd, R. . *J. Polym. Sci., Part B: Polym. Phys.* **1997**, *35*, 1135. Silvestri, R.; Sgarzi, P. *Polymer* **1998**, *39*, 5871. Chien, J. C. W.; Iwamoto, Y.; Rausch, M. D.; Wedler, W.; Winter, H. H. *Macromolecules* **1997**, *30*, 3447.

(23) Newman, S.; Cox, W. P. *J. Po1ym. Sci.* **1960**, *46*, 29.
(24) Mandelkern, L. *Crystallization of Polymers*; Cambridge University Press: New York, 2002; Vol. *I*.
(25) Auriemma, F.; De Rosa, C.; Boscato, T.; Corradini, P. *Macromolecules* **2001**, *34*, 4815. Auriemma, F.; De Rosa, C. *Macromolecules* **2002**, *35*, 9057.
(26) Brückner, S.; Meille, S. V. *Nature* **1989**, *340*, 455. Meille, S. V.; Brückner, S.; Porzio, W. *Macromolecules* **1990**, *23*, 4114.
(27) Keith, D. H.; Padden, F. J. *J. Appl. Phys.* **1964**, *35*, 1270. Keith, D. H.; Padden, F. J. *Polymer* **1986**, *27*, 1463. Keith, D. H.; Padden, F. J. *J. Polym. Sci.: Polym. Phys. Ed.* **1987**, *25*, 229.